MARTIN MARIETTA ENERGY SYSTEMS LIBRARIES
3 4456 0388822 9

127

ORNL-3973, Vol. II
UC-34 – Physics

NEUTRON PHYSICS DIVISION ANNUAL PROGRESS REPORT FOR PERIOD ENDING MAY 31, 1966

ORNL TECHNICAL INFORMATION DIVISION
Y-12 TECHNICAL LIBRARY
Document Reference Section
LOAN COPY ONLY
Do NOT transfer this document to any other person. If you want others to see it, attach their names, return the document, and the Library will arrange the loan as requested.
UCN-1624
(3 5-60)

OAK RIDGE NATIONAL LABORATORY
operated by
UNION CARBIDE CORPORATION
for the
U.S. ATOMIC ENERGY COMMISSION

Printed in USA. Price $2.00. Available from the Clearinghouse for Federal Scientific and Technical Information, National Bureau of Standards, U.S. Department of Commerce, Springfield, Virginia 22151

LEGAL NOTICE

This report was prepared as an account of Government sponsored work. Neither the United States, nor the Commission, nor any person acting on behalf of the Commission:

A. Makes any warranty or representation, expressed or implied, with respect to the accuracy, completeness, or usefulness of the information contained in this report, or that the use of any information, apparatus, method, or process disclosed in this report may not infringe privately owned rights; or

B. Assumes any liabilities with respect to the use of, or for damages resulting from the use of any information, apparatus, method, or process disclosed in this report.

As used in the above, "person acting on behalf of the Commission" includes any employee or contractor of the Commission, or employee of such contractor, to the extent that such employee or contractor of the Commission, or employee of such contractor prepares, disseminates, or provides access to, any information pursuant to his employment or contract with the Commission, or his employment with such contractor.

OK 11/21/67

ORNL 3973, Vol. II
Errata

NEUTRON PHYSICS DIVISION
ANNUAL PROGRESS REPORT
FOR PERIOD ENDING MAY 31, 1966

Please make the following changes in your copy of the subject report. On page 74, replace second column. On page 75, replace entire page. The attached copy is printed on gummed stock and may be cut out and pasted directly on the pages.

ORNL-3973, Vol. II

Contract No. W-7405-eng-26

NEUTRON PHYSICS DIVISION
ANNUAL PROGRESS REPORT
For Period Ending May 31, 1966

F. C. Maienschein, Director
A. D. Callihan, Associate Director

Group Leaders

C. E. Clifford, Reactor and Weapons Radiation Shielding
R. G. Alsmiller, Theoretical Space and High-Energy Accelerator Shielding
R. W. Peelle, Experimental Space and High-Energy Accelerator Shielding

SEPTEMBER 1966

MARTIN MARIETTA ENERGY SYSTEMS LIBRARIES
3 4456 0388822 9

OAK RIDGE NATIONAL LABORATORY
Oak Ridge, Tennessee
operated by
UNION CARBIDE CORPORATION
for the
U. S. ATOMIC ENERGY COMMISSION

Contents

7. THEORETICAL STUDIES FOR HIGH-ENERGY RADIATION SHIELDING 71

7.1 High-Energy Nucleon Transport and Space Vehicle Shielding – R. G. Alsmiller, Jr. 71

7.2 Calculations of Radiation Hazard Due to Exposure of Supersonic Jet Aircraft to Solar Flares – M. Leimdorfer, R. G. Alsmiller, Jr., and R. T. Boughner 71

7.3 Calculated Fluxes of Less than 50-MeV Neutrons Diffusing Beneath the Shield of a Meson Production Facility – W. E. Kinney 73

7.4 Electron-Photon Cascade Calculations and Neutron Yields from Electrons in Thick Targets – R. G. Alsmiller, Jr., and H. S. Moran 73

7.5 Shielding Calculations for High-Energy Accelerators – R. G. Alsmiller, Jr. 74

7.6 Transport of Very High Energy Muons Through Thick Shields – R. G. Alsmiller, Jr., M. Leimdorfer, and H. S. Moran 74

7.7 Proton Spectrum from Nuclear Collisions of 1.7-BeV/c Negative Pions in Emulsions – D. T. King 76

7.8 Radiochemical Cross Sections and the Effects of a Few Nuclear Parameters for Incident Protons and π^- Mesons in the 200-MeV Energy Region – H. W. Bertini 76

7.9 A Few Comparisons with Experiment Using Results from a Preliminary Calculation of Nucleon-Nucleus Reactions at About 700 MeV – H. W. Bertini 77

7.10 Analytic Representation of Nonelastic Cross Sections and Particle Emission Spectra from Nucleon-Nucleus Collisions in the Energy Range 25 to 400 MeV – R. G. Alsmiller, Jr., M. Leimdorfer, and J. Barish 78

7.11 Tissue Current-to-Dose Conversion Factors for Neutrons with Energies from 0.5 to 60 MeV – D. C. Irving, R. G. Alsmiller, Jr., and H. S. Moran 82

7.12 Method of Representing Two-Dimensional Distributions for Use in Monte Carlo Calculations – M. Leimdorfer and J. Barish 82

7.13 Energy Parameters for Light Nuclides in Monte Carlo Nuclear Evaporation Programs Based on EVAP – R. W. Peelle and P. M. Aebersold 82

7.14 Monte Carlo Study of Method for Lunar (Surface) Analysis Based on Spectroscopy of Gamma Rays Following 14-MeV Pulsed-Neutron Bombardment – M. Leimdorfer and R. T. Boughner 83

7.15 Space and Accelerator Shielding Information Collected by Radiation Shielding Information Center – R. G. Alsmiller, Jr., F. S. Alsmiller, and J. Gurney 83

8. EXPERIMENTAL STUDIES FOR HIGH-ENERGY RADIATION SHIELDING 85

8.1 Status of the 60-MeV Charged Reaction Particle Experiment – F. E. Bertrand, R. W. Peelle, T. A. Love, W. R. Burrus, N. W. Hill, and B. Rust 85

8.2 Proposed Measurements of Secondary Neutrons from Targets Bombarded by 600-MeV Protons – W. A. Gibson, J. W. Wachter, and V. V. Verbinski 86

8.3 Secondary Nucleon Energy Spectra from Targets Bombarded by High-Energy Protons – J. W. Wachter, W. R. Burrus, and W. A. Gibson 88

8.4 Secondary Gamma Rays from Proton and Alpha Bombardment of Light- to Medium-Weight Nuclei – W. Zobel, F. C. Maienschein, G. T. Chapman, and J. H. Todd 89

8.5 Beam Energy Measurements at the Oak Ridge Isochronous Cyclotron – R. T. Santoro, F. E. Bertrand, T. A. Love, and R. W. Peelle 92

8.6 Evaluation of QUIKTRAN Real Time Computer Terminal – W. R. Burrus 92

8.7 Measurements of (p,n) Neutron-Production Cross Sections for 18.5- and 15.1-MeV Protons on Be, N, Al, Fe, In, Ta, and Pb at Angles of 0 to 170° and Neutron Energies Above 0.8 MeV – V. V. Verbinski, W. R. Burrus, and M. Young 94

8.8 $^{9}Be(\alpha,n)$ Neutron-Production Cross Sections vs Neutron Energy and Angle for 6- to 10.5-MeV Alpha Particles – V. V. Verbinski, J. K. Dickens, W. E. Kinney, and F. G. Perey 95

9. RADIATION DETECTOR STUDIES (II) 96

9.1 Multiple Coulomb Scattering into a Detector in Charged-Particle Coincidence Measurements Between Reaction Products – R. W. Peelle 96

9.2 A Total-Absorption Detector for 60-MeV Protons Using Lithium-Drifted Germanium – F. E. Bertrand, R. W. Peelle, T. A. Love, R. J. Fox, N. W. Hill, and H. A. Todd 96

9.3 Temperature Dependence of the Response of Lithium-Drifted Germanium Detectors to Gamma Rays – M. M. El-Shishini and W. Zobel 97

9.4 Simultaneous Connection of Fast- and Slow-Amplifier Systems to Semiconductor Systems – N. W. Hill and R. W. Peelle 97

9.5 Response Function for Neutron Time-of-Flight Spectroscopy – R. T. Santoro and R. W. Peelle 100

9.6 Proton Recoil Spectrometer for Neutron Spectra Between 50 and 450 MeV – W. A. Gibson, W. R. Burrus, J. W. Wachter, and C. F. Johnson 102

7. Theoretical Studies for High-Energy Radiation Shielding

7.1 HIGH-ENERGY NUCLEON TRANSPORT AND SPACE VEHICLE SHIELDING[1]

R. G. Alsmiller, Jr.

Recent work on the transport of high-energy massive particles, protons, neutrons, alpha particles, etc., through dense matter as this work applies to the shielding of manned space vehicles is reviewed. The transport of heavy particles through tissue and the resultant physical dose (rads) are considered, but the important question of the biological effects of radiation is not discussed. Throughout the discussion an attempt is made to indicate the areas of uncertainty where further research is required and particularly to indicate the areas where experimental confirmation of theoretical results is needed.

References

[1]Abstract of ORNL-TM-1518 (1966); work funded by National Aeronautics and Space Administration under NASA order R-104(1).

7.2 CALCULATIONS OF RADIATION HAZARD DUE TO EXPOSURE OF SUPERSONIC JET AIRCRAFT TO SOLAR FLARES[1]

M. Leimdorfer R. G. Alsmiller, Jr.
R. T. Boughner[2]

Travelers and operating personnel in the proposed supersonic jet aircraft will, at least when traveling polar routes, be subject to a radiation hazard from solar protons and the secondary particles produced in the atmosphere by these protons.[3,4] To determine the magnitude of this hazard, a series of Monte Carlo calculations have been carried out giving estimates of the dose levels from a typical flare spectrum at various depths in the atmosphere.

The calculations were carried out using the nucleon transport code NTC, which uses an intranuclear cascade model to predict the energy and angular distributions of the nucleons emitted in high-energy nucleon-nucleus collisions.[5] The quality factors used to convert from rads to rems were taken to be the same as those used in the work of Zerby and Kinney.[6] The geometry was simplified to the case of multilayer slabs with the following composition (starting at the top of the atmosphere): X g of air per cm^2, 1 g of iron per cm^2, 30 g of tissue per cm^2, 1 g of iron per cm^2, and an infinite layer of air. The three middle layers were used to simulate the aircraft and the passengers.

The solar protons were assumed to be incident isotropically at the top of the atmosphere and were taken to have an integral spectrum exponential in rigidity; that is, the incident spectrum was taken to be of the form

$$N(>E) = N_0 e^{-P(E)/P_0} ,$$

where

$$P = \frac{1}{ze} [E(E + 2mc^2)]^{1/2} ,$$

z = charge number,

e = electronic charge,

E = kinetic energy,

m = mass,

c = velocity of light.

In the calculations P_0 was taken to be 100 MV, and the incident flux was normalized to 1 particle/cm^2 with energy greater than 30 MeV. Only

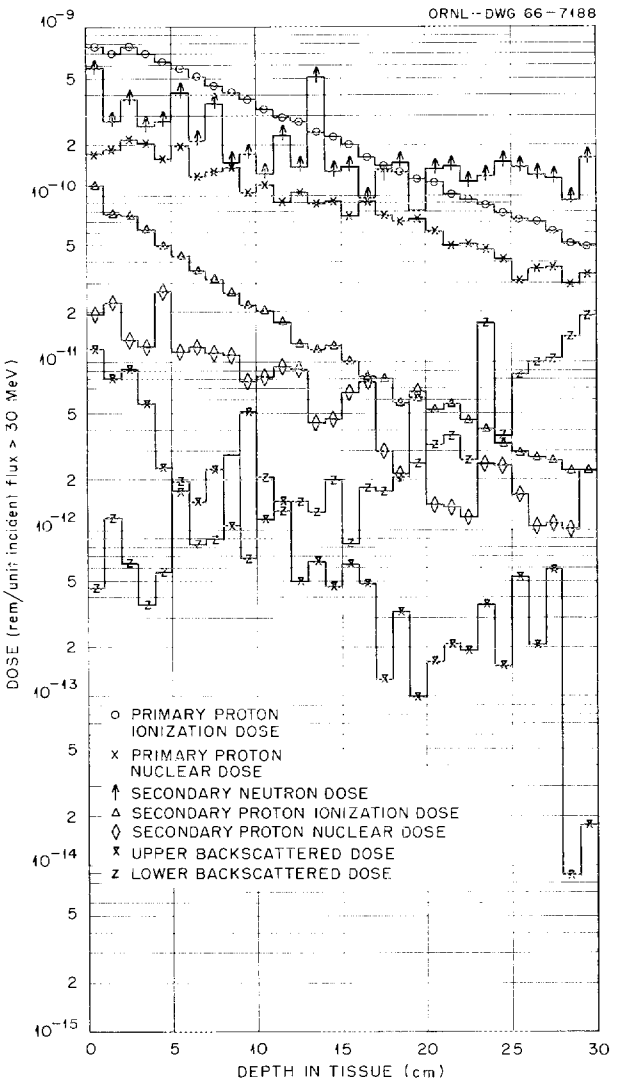

Fig. 7.2.1. Dose vs Depth in Tissue for Atmospheric Depth of 22 g/cm^2 (~85,000 ft).

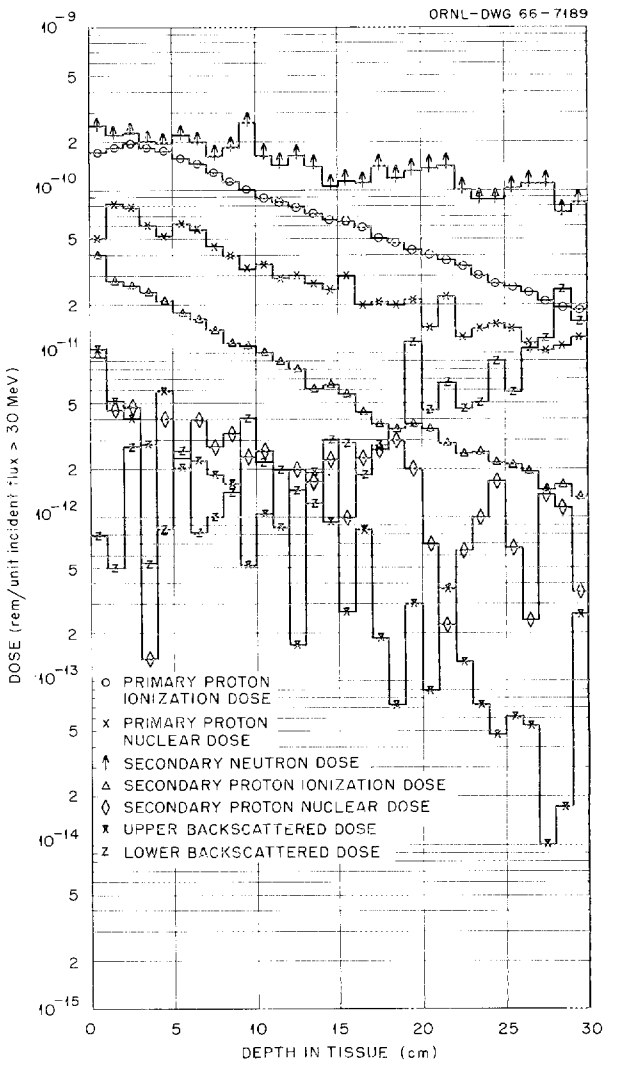

Fig. 7.2.2. Dose vs Depth in Tissue for Atmospheric Depth of 36 g/cm^2 (~75,000 ft).

incident protons with energies between 50 and 450 MeV were considered. The incident protons with energy less than 50 MeV are stopped in the air, and the few secondary particles from these low-energy protons may be neglected.[7] The particles above 450 MeV were not considered because of the lack of particle production data at the higher energies. This is, of course, a limitation on the calculations and does not mean that the contribution of the higher-energy incident particles is thought to be entirely negligible.

The rem dose as a function of depth in the tissue at three atmospheric depths, $X = 22$ g/cm^2 (~85,000 ft), $X = 36$ g/cm^2 (~75,000 ft), and $X = 58$ g/cm^2 (~65,000 ft), is shown in Figs. 7.2.1, 7.2.2, and 7.2.3 respectively. A variety of curves are given showing the various individual contributions to the dose. The total dose at each depth is obtained by adding all the individual contributions on a given graph. The various secondary fluxes are defined to be those that would exist at the upper shield-tissue interface if the tissue and everything below it were replaced by vacuum. The curves labeled "primary proton nuclear dose" and "secondary proton nuclear dose" represent the dose from all particles produced by nuclear col-

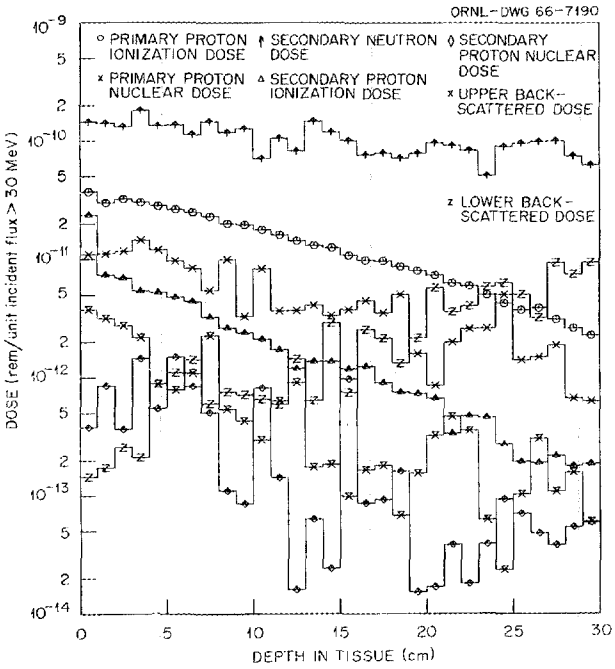

Fig. 7.2.3. Dose vs Depth in Tissue for Atmospheric Depth of 58 g/cm^2 (~65,000 ft).

lisions in the tissue of primary and secondary particles respectively. The upper backscattered dose is the dose from all particles and their progeny which cross from the tissue into the upper layer of iron. The lower backscattered dose is the dose from all particles and their progeny which cross from the lower iron layer into the tissue.

The secondary particles contribute appreciably to the dose at all depths considered.

References

[1]Work funded by National Aeronautics and Space Administration under NASA order R-104(1).

[2]Mathematics Division.

[3]A report of the ICRP Task Group, "Radiobiological Aspects of the Supersonic Transport," *Health Phys.* **12**, 209 (1966).

[4]E. J. Flamm and R. E. Lingenfelter, *Science* **144**, 1566 (1964).

[5]W. E. Kinney, *The Nucleon Transport Code, NTC*, ORNL-3610 (1964).

[6]C. D. Zerby and W. E. Kinney, *Nucl. Instr. Methods* **36**, 125 (1965).

[7]D. C. Irving *et al.*, *The Secondary Particle Contribution to the Dose from Solar Flare Protons Incident Isotropically on Slab Shields*, ORNL-TM-1210.

7.3 CALCULATED FLUXES OF LESS THAN 50-MeV NEUTRONS DIFFUSING BENEATH THE SHIELD OF A MESON PRODUCTION FACILITY[1]

W. E. Kinney

Fluxes of neutrons of energy less than 50 MeV which diffuse beneath an idealized shield for a meson production facility were estimated by Monte Carlo methods. Neutrons from a 400-MeV point isotropic source impinged on the shield configuration, where lower-energy neutrons were produced by intranuclear cascades. Neutrons below 50 MeV were then treated, and the fluxes were computed by statistical estimation. The fluxes at 0, 5, and 10 ft behind the shield were calculated to be $(2.7 \pm 0.8) \times 10^{-10}$, $(3.6 \pm 1.1) \times 10^{-11}$, and $(1.4 \pm 0.4) \times 10^{-11}$ neutron cm^{-2} (source neutron)$^{-1}$ respectively. The flux at 0 ft produces an average whole-body dose rate of 3.6 R/h.

References

[1]Abstract of ORNL-TM-1423 (Feb. 23, 1966).

7.4 ELECTRON-PHOTON CASCADE CALCULATIONS AND NEUTRON YIELDS FROM ELECTRONS IN THICK TARGETS[1]

R. G. Alsmiller, Jr. H. S. Moran

The electron-photon cascades induced in cylindrical targets of various sizes and materials by electrons in the energy range 30 to 200 MeV were studied, and calculations of the resulting neutron yields are presented. These calculated yields are compared with experimental yields, and approximate agreement is obtained.

References

[1]Submitted to *Nuclear Instruments and Methods;* also published as ORNL-TM-1502 (1966). Work partially funded by National Aeronautics and Space Administration under NASA order R-104(1).

7.5 SHIELDING CALCULATIONS FOR HIGH-ENERGY ACCELERATORS[1]

R. G. Alsmiller, Jr.

This is a review paper on existing high-energy-accelerator shielding calculations that was presented as an invited paper at the First Symposium on Accelerator Radiation Dosimetry and Experience, Brookhaven National Laboratory, November 3–5, 1965.

References

[1]Abstract of ORNL-TM-1298 (Oct. 14, 1965).

7.6 TRANSPORT OF VERY HIGH ENERGY MUONS THROUGH THICK SHIELDS

R. G. Alsmiller, Jr. M. Leimdorfer
H. S. Moran

One of the many shielding problems associated with high-energy accelerators, such as the proposed 200-GeV accelerator, is the shielding against mu mesons produced in the experimental area.[1] The general situation is that of a proton beam which interacts with a target to produce a variety of particles, including π mesons and κ mesons. After leaving the target, the produced particles travel through a drift space and then enter a shield. In traveling through the drift space, an appreciable fraction of the π and κ mesons decay into muons. The shielding thickness in the forward direction with respect to the proton beam is usually determined by the muons formed in the drift space; that is, the other particles which enter the shield may be neglected. Muons do not undergo strong interaction, and for energies of less than 50 to 100 GeV the primary mechanism of energy loss is the ionization and excitation of atoms.[2,3] Thus the shielding problem in the forward direction reduces to the transport of high-energy muons, taking into account only Coulomb interactions.

A Monte Carlo transport code for protons which includes only Coulomb interactions but takes into account range straggling and small-angle multiple scattering has recently been written by Johansson and Leimdorfer.[4,5] By making the appropriate changes in mass and stopping power, this code has been adapted to muon transport calculations.

In Figs. 7.6.1 and 7.6.2 the calculated lateral distribution of muons at depths of 30 and 55 m, respectively, for the case of 100-GeV muons normally incident on a cylindrical shield of iron 80 cm in radius is shown. The solid histograms show the lateral distribution of muons given by the Monte Carlo code, while the dashed histogram in Fig. 7.6.2 shows the lateral distribution of muons given by the code when range straggling is neglected. The solid curve marked "Eyges" shows the Gaussian distribution given by the approximate analytic theory of Eyges.[6] The solid curve marked "Moliere" is obtained using the approximate theory of Eyges but with a W^2 given by the multiple-scattering angular distribution of Moliere.[4] At a depth of 30 m, which is well below the range of the incident particles, range straggling has no appreciable effect on the lateral distribution. At a depth of 55 m, the lateral distribution is affected by range straggling. The number of muons per incident muon which reaches this depth in the target is 0.671 when range straggling is included and 0.643 when range straggling is neglected.

In addition to changing the number of particles which reach large depths, range straggling also changes markedly the energy distribution of the particles at a given depth. In Fig. 7.6.3 the energy distribution of the muons at a depth of 55 m is

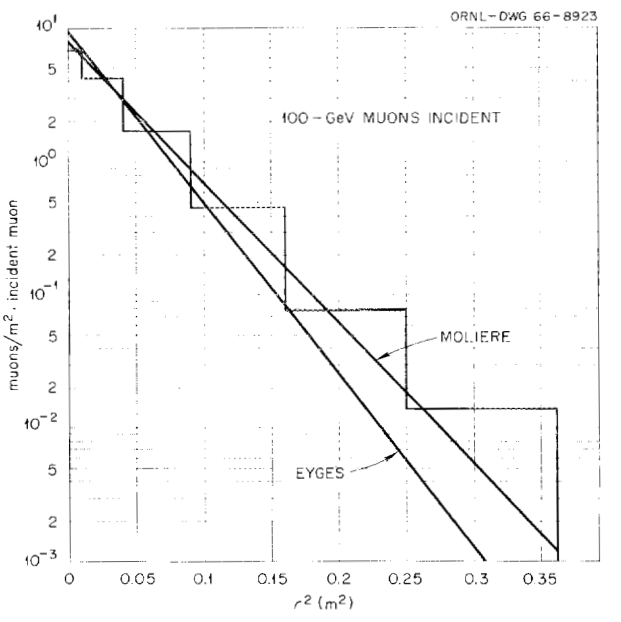

Fig. 7.6.1. Lateral Distribution of Muons at a Depth of 30 m in a Cylindrical Shield of Iron: 100-GeV Incident Muons.

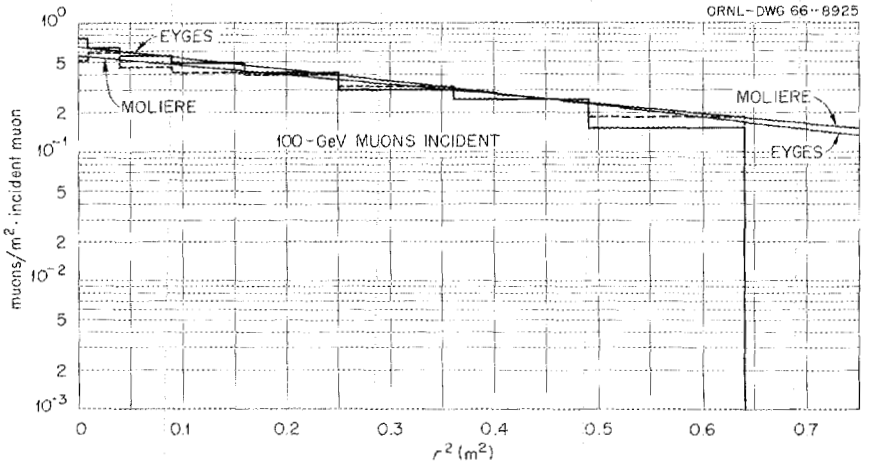

Fig. 7.6.2. Lateral Distribution of Muons at a Depth of 55 m in a Cylindrical Shield of Iron: 100-GeV Incident Muons.

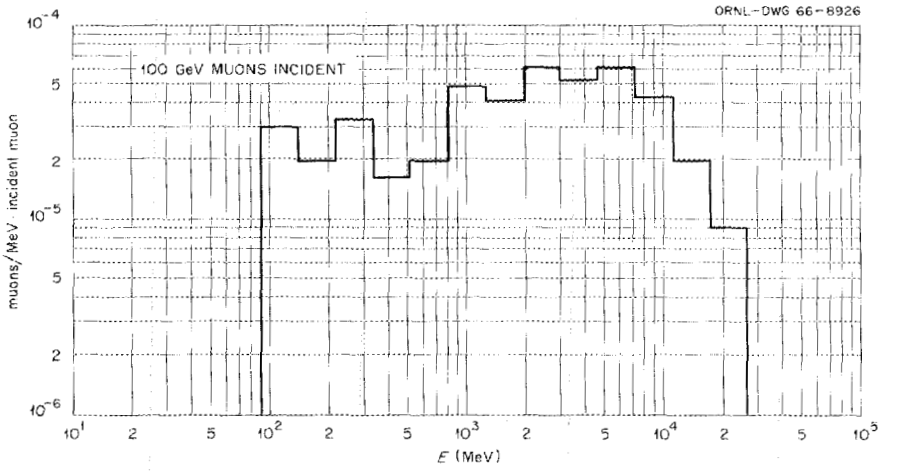

Fig. 7.6.3. Muon Energy Distribution at a Depth of 55 m in a Cylindrical Shield of Iron.

shown. Without range straggling, all the muons would arrive at this depth with an energy of approximately 1 GeV. One can specify only approximately the energy with which the particles would arrive at this depth, because even without straggling there is a slight spread in the energy distribution due to the different path lengths traveled by the various particles.

In the general accelerator shielding problem the muons incident on the shield have both an energy distribution and an angular distribution. The existing program is being modified so that calculations in this more general case may be carried out.

References

[1] *200-GeV Accelerator Design Study*, UCRL-16000, p. XII-25 (1965).

[2] P. J. Hayman, N. S. Palmer, and A. W. Wolfindale, *Proc. Roy. Soc. (London)* **275A**, 391 (1963).

[3] R. W. Thomas, *Energy Loss of High Energy Muons*, UCID-10010.

[4] C. Johansson and M. Leimdorfer, *A Monte Carlo Procedure for Calculating the Migration of Protons Taking Account Only of Electromagnetic Interactions*, Forsvarets Forskningsanstalt, Stockholm, FOA 4, Rapport A4411-411 (1965).

[5] C. Johansson, *Program Description and Users Manual for Protons, A Computer Program for Treating Proton Slowing-Down Due to Atomic Collisions*, Forsvarets Forskningsanstalt, Stockholm, FOA 4, Rapport A4436-411 (1965).

[6] L. Eyges, *Phys. Rev.* **74**, 1534 (1948).

7.7 PROTON SPECTRUM FROM NUCLEAR COLLISIONS OF 1.7-BeV/c NEGATIVE PIONS IN EMULSIONS

D. T. King[1]

Observations have been made on the tracks of charged particles emergent from 800 nuclear collisions made in a stack of Ilford K5 emulsions by a beam of 1.7-BeV/c negative pions from the Lawrence Radiation Laboratory bevatron. The nuclear collisions may be distinguished provisionally as occurring in heavy (Ag, Br) or light (C, N, O) nuclei, dependent on the number N_h of evaporation prongs; for Ag and Br, $N_h \geqq 6$. From a calibration of ionization on the tracks of particles of known energy in the stack, the relation between grain density, g, and velocity, $v = \beta C$, in the range $0.5 \leqq \beta \leqq 0.8$ has been established. For emergent particles with track lengths in the emulsion exceeding 3.0 mm and velocities in this range, the protons can then be distinguished from pions through an evaluation of the multiple Coulomb scattering.[2] The energies and polar angles of emission of 30 protons projected from π^- collisions with Ag and Br nuclei have been measured, and the data are presented in the form of an energy vs angle scatter diagram in Fig. 7.7.1. These data may be compared with the predictions of nucleon emission derived from Monte Carlo calculations of the intranuclear cascade produced in intermediate nuclei by energetic pions.[3]

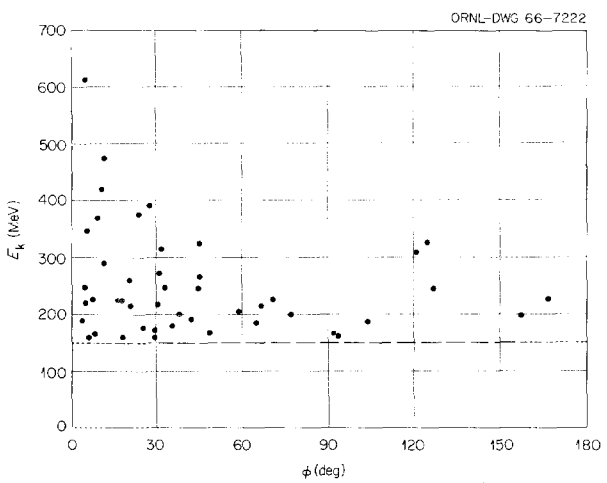

Fig. 7.7.1. Energy of Protons Projected from π^- Collisions with Ag and Br Nuclei as a Function of the Polar Angle of Emission.

References

[1]Consultant, University of Tennessee.

[2]C. F. Powell, P. H. Fowler, and D. H. Perkins, *The Study of Elementary Particles by the Photographic Method*, p. 114, Pergamon, New York, 1959.

[3]H. W. Bertini, private communication.

7.8 RADIOCHEMICAL CROSS SECTIONS AND THE EFFECTS OF A FEW NUCLEAR PARAMETERS FOR INCIDENT PROTONS AND π^- MESONS IN THE 200-MeV ENERGY REGION[1]

H. W. Bertini

Theoretical predictions were made for the cross sections of a few $(p,xpyn)$ reactions on C, Al, Cu, and U targets in the energy range 50 to 400 MeV and compared with experimental results. A two-step cascade-evaporation calculation was used in which the diffuse nuclear surface was taken into account. The results indicated that agreement to within about 40% can be expected when the reaction cross section is about 100 mb, but that the agreement can be no better than by a factor of 3 when the cross section is about 10 mb. A comparison with experiment for the (π^-,π^-n) reaction on carbon was made over the energy range 50 to 300 MeV, and the agreement was found to be fair when the diffuse nuclear surface was included. A method is suggested which differs from the usual method for measuring the real part of the optical-model potential for pions on carbon by making use of the position of the peak in the cross section for the (π^-,π^-n) reaction vs energy.

It is shown that the effect of increasing the radius used in the calculation of the (p,pn) cross section on carbon is more prominent than the effect of changing the nucleon density distribution for a given radius. Finally, results are given for the dependence of the $(p,xpyn)$ cross sections on the transition energy used in the calculation between the cascade and evaporation processes, which led to the conclusion that the lowest transition energy gives the results most consistent with experiment.

References

[1]Abstract of paper to be submitted to the *Physical Review;* work partially funded by National Aeronautics and Space Administration under NASA order R-104(1).

7.9 A FEW COMPARISONS WITH EXPERIMENT USING RESULTS FROM A PRELIMINARY CALCULATION OF NUCLEON-NUCLEUS REACTIONS AT ABOUT 700 MeV[1]

H. W. Bertini

The intranuclear cascade calculation for incident particle energies from 25 MeV to 2 GeV previously reported[2] is continuing to undergo debugging. The program is in operation, however, and a few very preliminary results have been compared with experiment, as illustrated in Figs. 7.9.1–7.9.3. They indicate a fair agreement with experiment, which is encouraging.

The free-particle cross sections of all types that are needed in the program are being brought up to date. Concurrently the separate isobar program is nearing completion. This program consists of that part of the cascade calculation which describes the production of pions[3] in the particle-particle collisions that occur inside the nucleus.

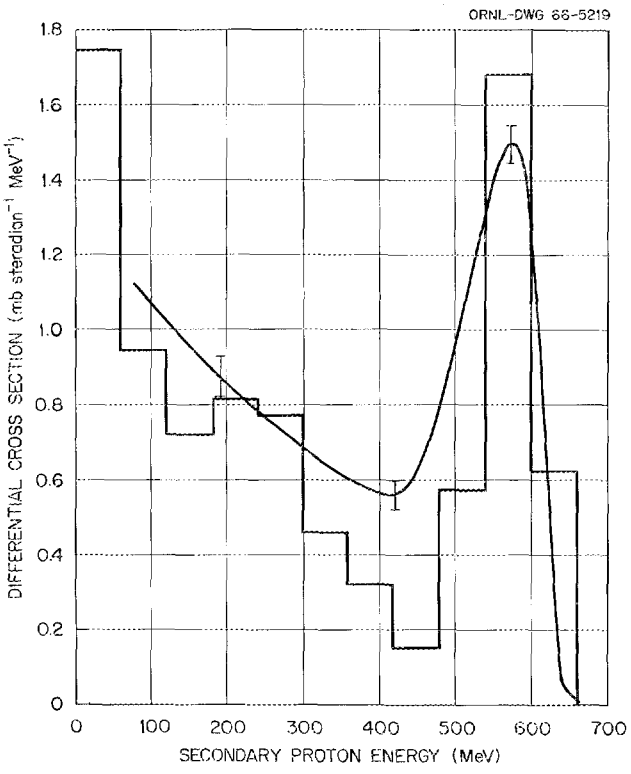

Fig. 7.9.1. Proton Energy Spectrum at 18° from 660-MeV Protons on Copper. Dashed lines: experimental results [L. S. Azhgirey *et al.*, *Nucl. Phys.* 13, 258 (1959)]; solid-line histogram: calculated spectrum for protons emitted into the angular interval 13 to 23°.

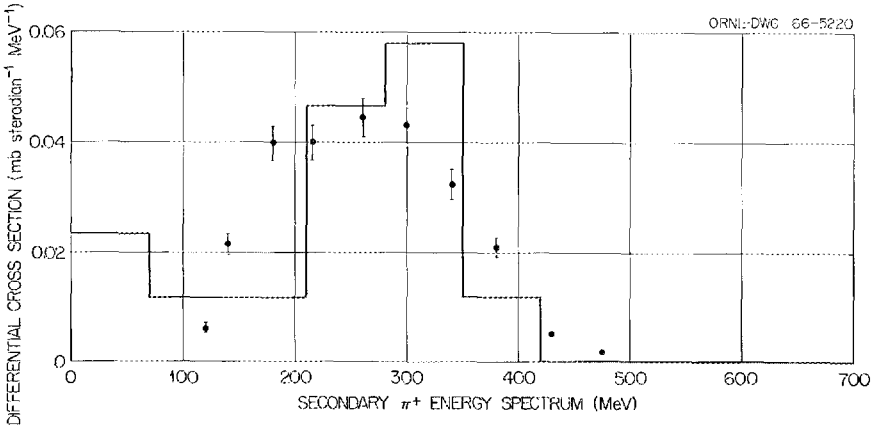

Fig. 7.9.2. Secondary π^+ Energy Spectrum at 0.349° from 725-MeV Protons on Carbon. Points show experimental results [R. P. Haddock (UCLA), M. Zeller (UCLA), and K. M. Crowe (UCRL), *Production of Charged Pions from Complex Nuclei in the Forward Direction*, unpublished; received Jan. 4, 1965]; solid-line histogram: calculated spectrum for π^+ emitted into the angular interval 0 to 10° from 700-MeV protons on carbon.

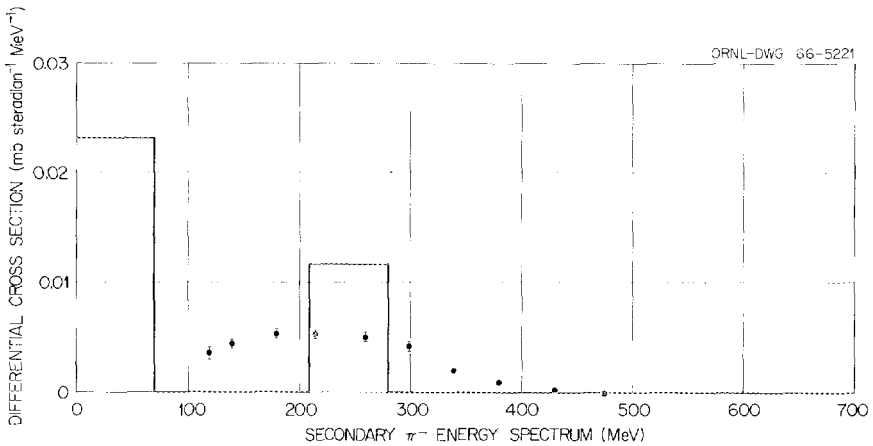

Fig. 7.9.3. Secondary π^- Energy Spectrum at 0.349° from 725-MeV Protons on Carbon. Points show experimental results [R. P. Haddock (UCLA), M. Zeller (UCLA), and K. M. Crowe (UCRL), *Production of Charged Pions from Complex Nuclei in the Forward Direction*, unpublished; received Jan. 4, 1965]; solid-line histogram: calculated spectrum for π^- emitted into the angular interval 0 to 10° from 700-MeV protons on carbon.

The program will be used to determine the accuracy of the model used to describe the production processes and to help in determining the angular distribution of the isobars.[4]

References

[1]Work partially funded by National Aeronautics and Space Administration under NASA order R-104(1).

[2]H. W. Bertini, *Neutron Phys. Div. Ann. Progr. Rept. Aug. 1, 1965,* ORNL-3858, vol. II, p. 80.

[3]H. W. Bertini, *Neutron Phys. Div. Space Radiation Shielding Research Ann. Progr. Rept. Aug. 31, 1962,* ORNL-CF-10-29, rev., p. 92.

[4]R. M. Sternheimer and S. J. Lindenbaum, *Phys. Rev.* **123**, 333 (1961).

7.10 ANALYTIC REPRESENTATION OF NONELASTIC CROSS SECTIONS AND PARTICLE EMISSION SPECTRA FROM NUCLEON-NUCLEUS COLLISIONS IN THE ENERGY RANGE 25 TO 400 MeV[1]

R. G. Alsmiller, Jr. M. Leimdorfer
J. Barish[2]

Using an intranuclear cascade model, Bertini has generated a large amount of data on the nonelastic cross section and the energy and angular distribution of emitted neutrons and protons when neutrons and protons in the energy range 25 to 400 MeV are incident on a variety of targets.[3-7] The calculations are carried out by Monte Carlo methods, and the data are presented in the form of histograms which, of course, contain statistical fluctuations. In order to make this large amount of data more accessible and, insofar as possible, to remove the statistical fluctuations, the data have been fitted by the method of linear least squares.

For both protons and neutrons in the energy range 25 to 400 MeV incident on the elements C, O, Al, Cr, Cu, Ru, Ce, W, Pb, and U, analytic expressions are given for

1. the nonelastic cross section as a function of energy,
2. the cascade[8] neutron and proton emission spectra in the angular intervals 0 to 30°, 30 to 60°, 60 to 90°, and 90 to 180°,
3. the evaporation[8] neutron and proton emission spectra (assumed isotropic),
4. the cascade neutron and proton emission spectra integrated over all angles.

The cascade emission spectra integrated over all angles can be obtained by summing the emission spectra in the individual angular intervals. This procedure, however, leads to functions which

involve many more parameters than are necessary; so separate fits for the angle-integrated spectra have been obtained.

Both the nonelastic cross section and all particle spectra have been represented by functions of the form

$$\exp\left(\sum_{j=0}^{\nu} a_j E^j\right),$$

and the coefficients have been obtained by minimizing the sum of the squares of the difference between the logarithm of the Monte Carlo data points and the expression

$$\sum_{j=0}^{\nu} a_j E^j .$$

In fitting the cross section, $\nu = 4$ was, in general, used. In fitting the emission spectra, ν was taken

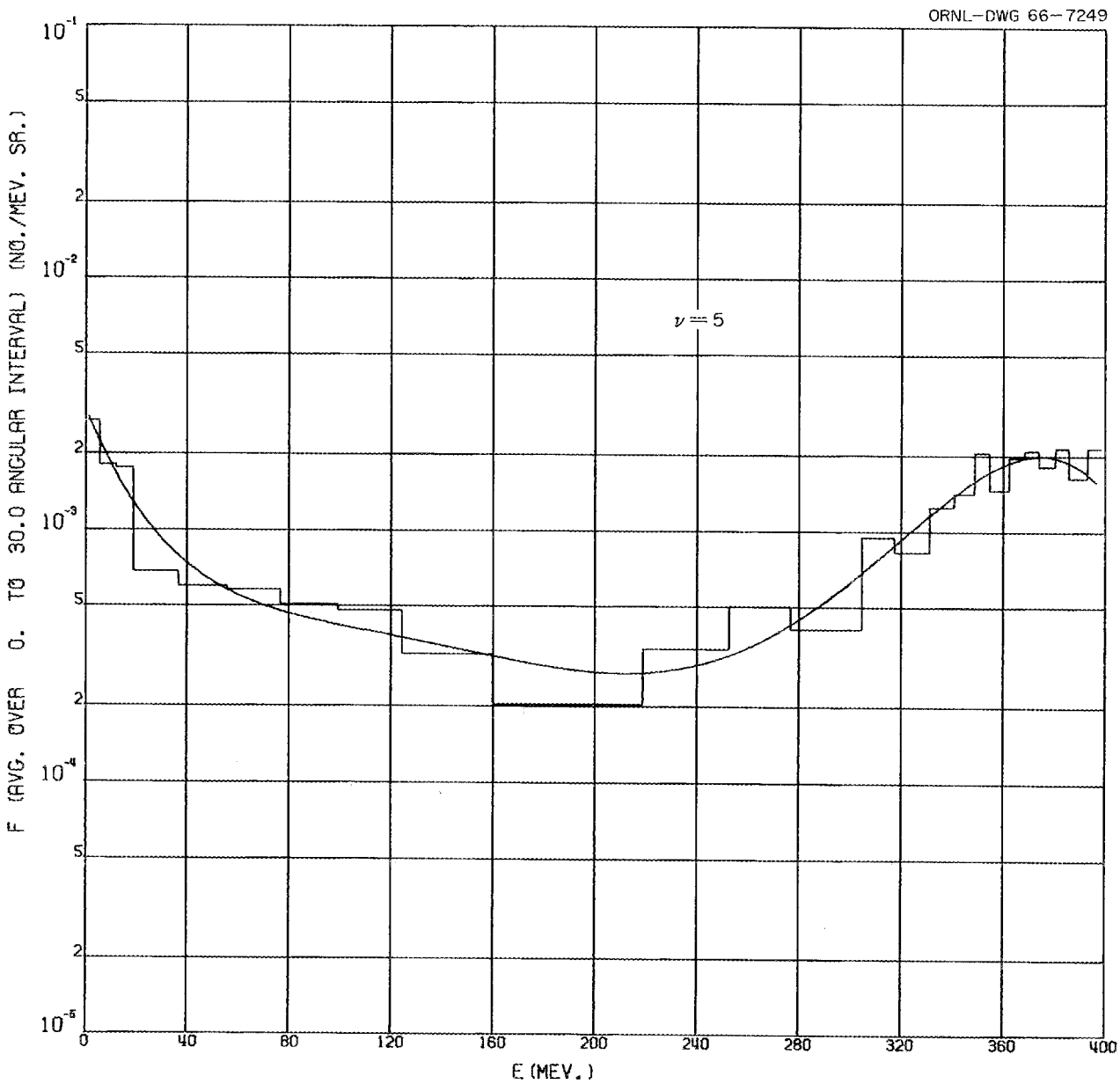

Fig. 7.10.1. Cascade Neutrons (Averaged over 0 to 30°) from 400-MeV Protons Incident on Aluminum: Comparison of Monte Carlo Histogram and Least-Squares Fit.

to be 5 or to be the number of Monte Carlo histogram intervals minus 2 when there were less than seven intervals.[9] In many cases, however, this large number of parameters led to unphysical oscillations in the analytic functions. When this occurred, the value of ν was systematically reduced until a function which did not oscillate excessively was obtained.

Comparisons between the Monte Carlo histograms and the fitted curves are shown in Figs. 7.10.1–7.10.3. The cascade neutrons from 400-MeV protons on aluminum averaged over an angular interval of 0 to 30° and integrated over all angles are shown in Figs. 7.10.1 and 7.10.2 respectively. The evaporation neutrons from 400-MeV protons on aluminum are shown in Fig. 7.10.3.

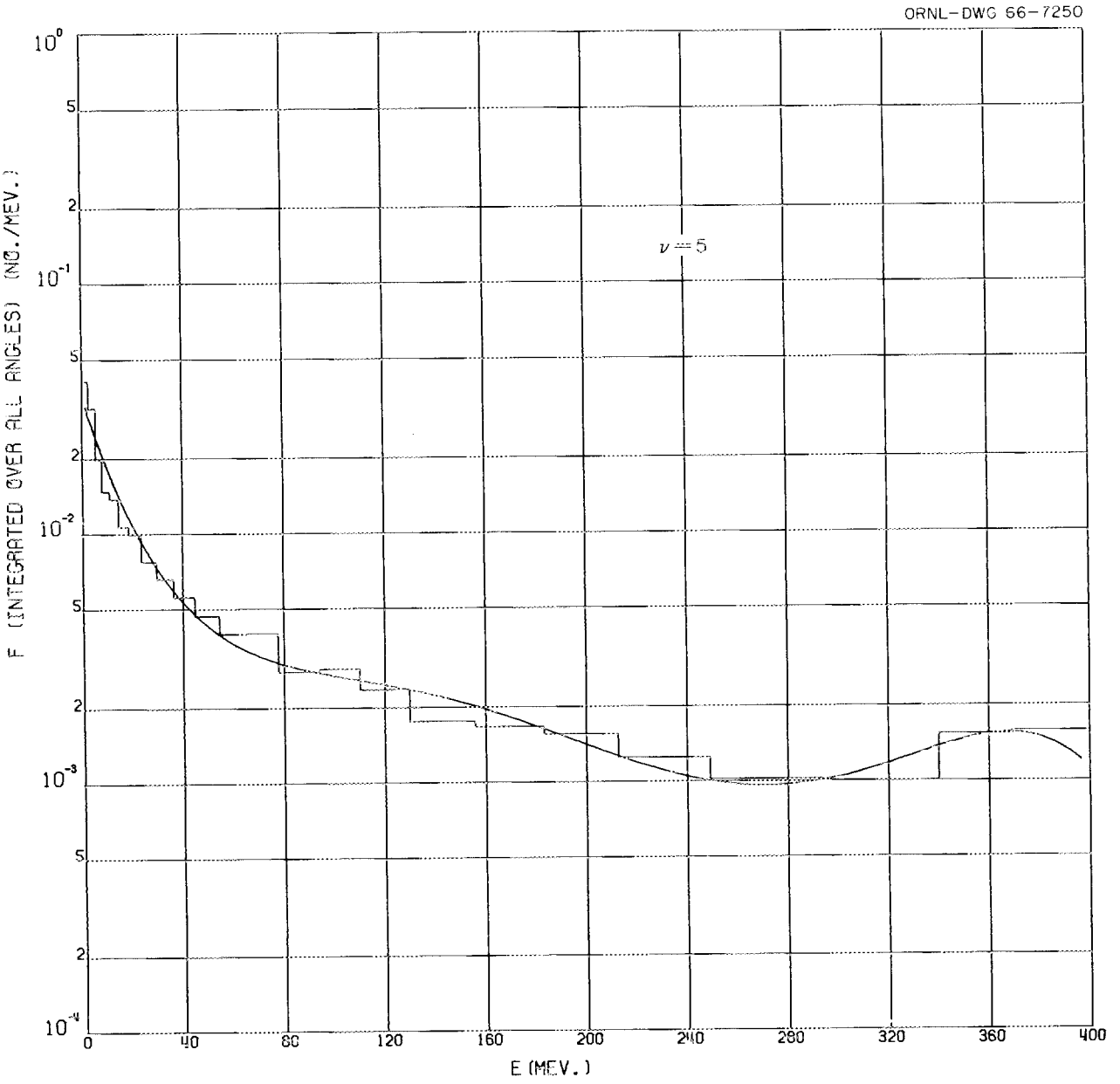

Fig. 7.10.2. Cascade Neutrons (Integrated over All Angles) from 400-MeV Protons Incident on Aluminum: Comparison of Monte Carlo Histogram and Least-Squares Fit.

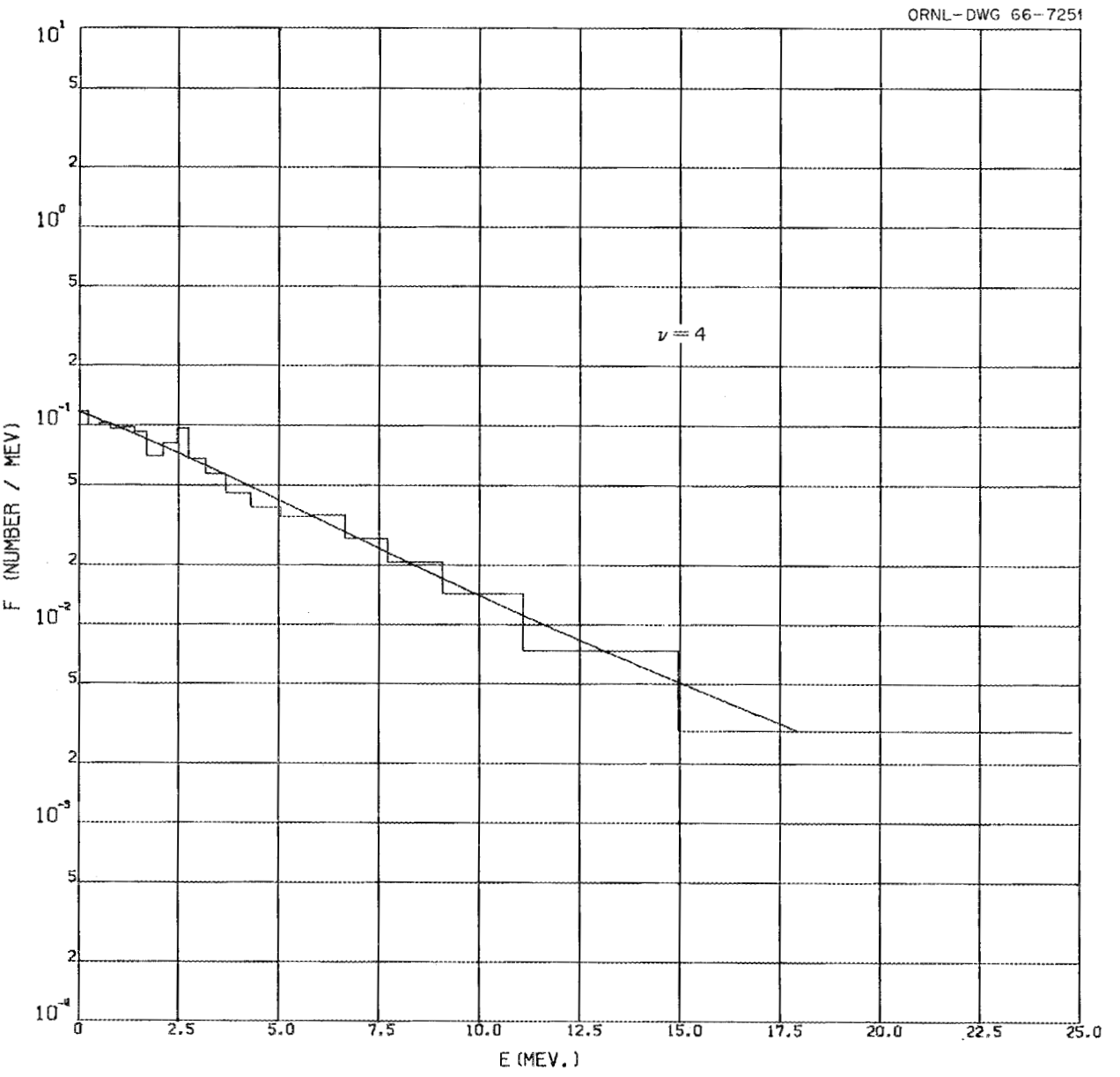

Fig. 7.10.3. Evaporation Neutrons from 400-MeV Protons on Aluminum: Comparison of Monte Carlo Histogram and Least-Squares Fit.

References

[1]Work partially funded by National Aeronautics and Space Administration under NASA order R-104(4).

[2]Central Data Processing Facility, Oak Ridge Gaseous Diffusion Plant.

[3]H. W. Bertini, *Phys. Rev.* **131**, 1801 (1963) with erratum *Phys. Rev.* **138**, AB2 (1965).

[4]H. W. Bertini, *Results from Low-Energy Intranuclear Cascade Calculations*, ORNL-TM-1225 (1965).

[5]H. W. Bertini, H. E. Francis, and M. P. Guthrie, *Instructions for the Operation of Codes Associated with the Low-Energy Intranuclear Cascade Calculation*, ORNL-3844 (in publication).

[6]W. A. Gibson *et al.*, "Comparison of Measured Neutron and Proton Spectra with Calculated Spectra

in the Energy Region Between 50 and 160 MeV," *Proceedings of the Second Symposium on Protection Against Radiations in Space, Oct. 12--14, 1964,* Gatlinburg, Tennessee, NASA SP-71, 337 (1965).

[7]H. W. Bertini, "Energy Spectra from Inelastic Nuclear Reactions at Energies Below 450 MeV," *Transactions of the 1965 Winter Meeting of the American Nuclear Society, Washington, D.C.* (This paper will be published in the proceedings of the special session on accelerator shielding at this meeting.)

[8]See ref. 3 for a discussion of the distinction between cascade and evaporation particles.

[9]The particle emission spectra presented by Bertini are in the form of histograms with equal energy intervals. The equal energy intervals were found to be inconvenient for fitting purposes; so before the fitting was carried out, the Monte Carlo history tapes were reanalyzed to produce a histogram with unequal energy intervals but with an equal number of emitted particles in each energy interval.

7.11 TISSUE CURRENT-TO-DOSE CONVERSION FACTORS FOR NEUTRONS WITH ENERGIES FROM 0.5 TO 60 MeV[1]

D. C. Irving R. G. Alsmiller, Jr.
H. S. Moran

To assist in the evaluation of the hazard associated with exposure to high-energy neutrons, a Monte Carlo computer program was used to calculate the energy deposition as a function of depth in a 30-cm-thick slab of tissue resulting from neutrons incident on the slab at energies up to 60 MeV. The program treated nonelastic and elastic interactions, including evaporation processes and nuclear recoils. Cases of both normal and isotropic incidence were calculated for neutrons of 0.5, 2, 10, 18, 30, and 60 MeV. From these data, current-to-dose conversion factors were extracted for the average whole-body dose, the dose at a 5-cm depth, and the maximum doses. A set of quality factors was adopted for transforming rad dose to rem dose.

References

[1]Abstract of ORNL-TM-1522 (to be published); work partially funded by National Aeronautics and Space Administration under NASA order R-104(1).

7.12 METHOD OF REPRESENTING TWO-DIMENSIONAL DISTRIBUTIONS FOR USE IN MONTE CARLO CALCULATIONS[1]

M. Leimdorfer J. Barish[2]

In an attempt to increase the efficiency of an existing Monte Carlo program, the Nucleon Transport Code (NTC),[3] for treating the transport of high-energy nucleons in matter, a method has been developed which is intended to improve the procedure for selecting combinations of the energy and angle of particles released in nuclear interactions. In the present form of NTC, the process of particle emission from nucleon-nucleus collisions is simulated by a Monte Carlo treatment of the intranuclear cascade. In the proposed method, the particle emission data obtained from the intranuclear cascade calculations are represented in the form of tables which are suitable for sampling purposes. The power of the method lies in the fact that the tables are constructed directly from the intranuclear cascade (Monte Carlo) histories.

References

[1]Abstract of ORNL-4002 (to be published); work partially funded by National Aeronautics and Space Administration under NASA order R-104(1).

[2]Central Data Processing Facility, Oak Ridge Gaseous Diffusion Plant.

[3]W. E. Kinney, *The Nucleon Transport Code, NTC,* ORNL-3610 (1964).

7.13 ENERGY PARAMETERS FOR LIGHT NUCLIDES IN MONTE CARLO NUCLEAR EVAPORATION PROGRAMS BASED ON EVAP[1]

R. W. Peelle P. M. Aebersold

The Monte Carlo nuclear evaporation system (EVAP) employed to estimate particle spectra

and radiochemical yields following calculated intranuclear cascade reactions has been modified, largely to improve the energy parameters for nuclides lighter than sodium. Additional nuclear masses have been added to the mass table for light nuclides, and the Cameron mass function is employed to give the mass difference between the unknown mass and a nearby known one. For nuclides having neutron or proton numbers less than 10, originally omitted correction parameters were added in the mass function for shell and pairing effects. Pairing energy corrections were similarly supplied in these cases for the level density estimation. Nuclei that are unstable to particle emission are not allowed to be residual nuclei, and when a nominal residual nucleus is also one of the possible evaporated particles, it is included in the spectrum of that particle without any residual excitation. The kinetic energy of each recoil nucleus is accumulated with the approximation of evaporation at 90° in the center-of-mass system. The effects of these changes are discussed, with typical results used as illustration. Except for the recoil calculation the changes had more impact on estimated radiochemical yields than on predicted particle spectra. Some radiochemical yield estimates were altered by a factor of more than 10.

References

[1]Abstract of ORNL-TM-1538 (to be published); work funded by the National Aeronautics and Space Administration under NASA order R-104(1).

7.14 MONTE CARLO STUDY OF METHOD FOR LUNAR (SURFACE) ANALYSIS BASED ON SPECTROSCOPY OF GAMMA RAYS FOLLOWING 14-MeV PULSED-NEUTRON BOMBARDMENT[1]

M. Leimdorfer R. T. Boughner[2]

In an investigation of the feasibility of analyzing the surface of the moon by gamma-ray spectroscopy techniques, Monte Carlo calculations were performed to estimate the spectral intensities of neutron-induced photons leaking from the moon surface during various time intervals following a burst of 14-MeV neutrons onto the surface. Four sets of calculations were done, all based on the lunar surface composition given by Urey and Craig,[3] with varying amounts of carbon and hydrogen (or deuterium) added. The four spectra for the time interval 0 to 10^{-6} sec following the burst are all essentially the same, clearly showing the inelastic de-excitation gamma rays from O, Si, Mg, and Fe, and also from C when that element was present. The spectra for later time intervals (10^{-6} to 10^{-5} sec, 10^{-5} to 10^{-4} sec, and 10^{-4} to 10^{-3} sec) are predominantly capture spectra dominated by iron capture gamma lines at 6.0 and 7.63 MeV and by the 2.23-MeV hydrogen capture gamma line when hydrogen was present. An examination of all the spectra indicates that, providing proper calibrations are made, the abundances of the various isotopes present on the lunar surface can be determined by gamma-ray spectroscopy techniques.

References

[1]Abstract of ORNL-TM-1446 (March 1966); work partially funded by National Aeronautics and Space Administration under NASA order R-104(1).

[2]Mathematics Division.

[3]H. C. Urey and H. Craig, *Geochim. Cosmochim. Acta* 4, 36 (1953).

7.15 SPACE AND ACCELERATOR SHIELDING INFORMATION COLLECTED BY RADIATION SHIELDING INFORMATION CENTER[1]

R. G. Alsmiller, Jr. F. S. Alsmiller
J. Gurney[2]

The collection of literature on shielding from radiation occurring in space and near accelerators was continued, and a bibliography was issued (ORNL-RSIC-11).[3] A collection of the abstracts of the literature covered in the bibliography was published as ORNL-RSIC-12.[4] A new service consisting of the automatic and selective dissemination of the literature was initiated, so that persons who provided RSIC with their field-of-

interest profiles were alerted as relevant literature of space and accelerator shielding was placed in the system.

References

[1]Work partially funded by National Aeronautics and Space Administration under NASA order R-104(10). All the RSIC work which is general to all shielding, including space, is discussed in sect. 4.

[2]Central Data Processing Facility, Oak Ridge Gaseous Diffusion Plant.

[3]R. G. Alsmiller, Jr., F. S. Alsmiller, and J. Gurney, *Bibliography, Subject Index, and Author Index of the Literature Examined by the Radiation Shielding Information Center (Space and Accelerator Shielding)*, ORNL-RSIC-11 (November 1965).

[4]*Abstracts of the Literature Examined by the Radiation Shielding Information Center (Space and Accelerator Shielding)*, ORNL-RSIC-12 (n.d.).

8. Experimental Studies for High-Energy Radiation Shielding

8.1 STATUS OF THE 60-MeV CHARGED REACTION PARTICLE EXPERIMENT[1]

F. E. Bertrand[2] W. R. Burrus
R. W. Peelle N. W. Hill[3]
T. A. Love B. Rust[4]

An experiment has been proposed to study the mass and energy spectrum of charged particles produced by bombardment of targets by ~60-MeV protons.[5] It is the purpose of this summary to describe the current status of the experiment.

In general, nearly all physical, electronic, and detector systems are complete, and it is expected that preliminary data leading to charged-particle cross sections will be obtained by late summer. Several days of cyclotron time have been used to test the detector and electronic systems. A description of the status of the various components follows.

An existing 48-in.-diam scattering chamber has been extensively modified to suit the needs of this experiment. The chamber, now in use, contains the following features: two remotely rotatable detector tables, a multiple target holder with remotely adjustable angle, a beam level port at +20° used for continuous scattered beam monitoring with an NaI(Tl) detector and a beam level port at −20° used for continuous beam energy monitoring using a range wheel,[6] a collimator design such that approximately 6° minimum scattering angle may be safely studied, a Faraday cup for beam intensity monitoring, and a coaxial beam pickoff for beam pulse monitoring and for timing signals.

As was previously reported, the detector system consists of two thin silicon ΔE detectors and a germanium total-absorption detector. An energy resolution of 0.2 to 0.3% and a peak-to-total ratio of ~0.94 for 60-MeV protons have been obtained using two different lithium-drifted germanium detectors. The details of the use of such detectors for intermediate-energy protons are reported elsewhere.[7] The detector is held in a "cold finger" mount which cools the detector to ~85°K and allows a covering over the detector of only 2 mg/cm^2 of nickel. The nickel is the only dead layer in the beam other than 2 mg/cm^2 of germanium dead layer. Two ΔE counters, a 500- and a 200-μ silicon surface-barrier detector, have been obtained which give resolution of less than 40 keV for 5-MeV alpha particles when operating at over twice depletion voltage.

Collimation for the detector system is provided by a 0.375- by 0.120-in. slit in a 1-mm-thick piece of NE-102 organic scintillator which serves as an anticoincidence detector. The entire detector system is mounted on a rotating table such that a 50-cm flight path is available and such that the spacing between detectors is a minimum to reduce multiple scattering losses.

The logic system is designed to use both fast and slow signals from all detectors. The fast signals will be used for all coincidence and anticoincidence gating. All fast amplifiers (which have a rise time as fast as 1 nsec) and slow transistor preamplifiers are mounted inside the vacuum chamber. Design of these units is well advanced, and models have been tested under experimental conditions and found to have stable gain in vacuum (drift from slow system <0.1%). Nearly all fast- and slow-logic components have been tested.

The data acquisition system consists of two 2048-channel analyzers and one 512-channel and one 256-channel analyzer. The over 40 bits of information available are read through an appropriate interface into a PDP-8 computer which will do preliminary analysis, write data on IBM-compatible magnetic tape, and give various on-line displays. The computer has been in use for a few months,

and at present the 2048-channel analyzers are interfaced with the computer and in use.

References

[1]Work funded by the National Aeronautics and Space Administration under NASA order R-104(1).

[2]Oak Ridge Graduate Fellow from Louisiana State University under appointment from the Oak Ridge Associated Universities.

[3]Instrumentation and Controls Division.

[4]Control Data Processing Facility, Oak Ridge Gaseous Diffusion Plant.

[5]F. E. Bertrand *et al.*, *Neutron Phys. Div. Ann. Progr. Rept. Aug. 1, 1965,* ORNL-3858, vol. II, p. 85.

[6]R. T. Santoro *et al.*, *Beam Energy Measurements at the Oak Ridge Isochronous Cyclotron,* ORNL-TM-1382 (Jan. 13, 1966).

[7]F. E. Bertrand *et al.*, *A Total-Absorption Detector for 60-MeV Protons Using Lithium-Drifted Germanium,* ORNL-TM-1462 (March 1966); *IEEE Proceedings of the 10th Annual Scintillation Semiconductor Detector Symposium* (to be published).

8.2 PROPOSED MEASUREMENTS OF SECONDARY NEUTRONS FROM TARGETS BOMBARDED BY 600-MeV PROTONS[1]

W. A. Gibson J. W. Wachter
V. V. Verbinski

As an extension of the program at ORNL to study the secondary nucleon production in the interaction of medium-energy protons with complex nuclei, an experiment to measure neutrons produced by 600-MeV protons on complex nuclei is being planned for the NASA cyclotron at Langley, Virginia. This experiment will be divided into two parts: measurement of neutron spectra at small angles, 0 to 5°, in the energy range 100 to 600 MeV and of neutron spectra at several angles between 0 and 150° in the energy range 2 to 50 MeV. Since the primary purpose of these experiments is to provide data to make comparisons with the ORNL Monte Carlo calculations of cross sections, the angle and energy regions were chosen to provide data in the areas where the calculations, up to this time, have had the least verification. Several targets, approximately 10 g/cm^2 thick, from carbon to bismuth will be used.

The high-energy neutron measurements will be made as indicated in Fig. 8.2.1. The 600-MeV proton beam will be focused on a target and, after passing through the target, will be bent by magnet *A* into a beam dump. The neutrons emitted at small angles will pass into the hydrogenous radiator, and a small fraction will produce recoil protons with an energy (ignoring mesons)

$$E_p = \frac{E_n \cos^2 \theta}{1 + (E_n/2Mc^2) \sin^2 \theta} ,$$

where E_p and E_n are the energy of the proton and neutron, respectively, M is the mass of the nucleon, and θ is the angle between the path of the incident neutron and recoiling proton. The protons recoiling at small angle will be focused by the quadrupole and bending magnet *B* on counter 3. The degree of bending by magnet *B* will be a measure of the recoil proton energy. Counter 2 will be placed in coincidence with counter 3 to reduce background counts. Counter 1 will be placed in anticoincidence with counters 2 and 3 to reject charged particles entering the radiator. The energy resolution of the system will be about 5%. Positrons and mesons with the same momentum as the protons will also be focused on counter 3. These lighter particles will be separated from the protons by dE/dx separation in the last counter.

If the measurements prove to be satisfactory, measurements at larger angles will be attempted.

The neutrons in the energy region between 2 and 50 MeV will be studied by recording the pulse-height spectra produced by recoil protons in a liquid organic scintillator. The neutron spectra will be obtained from the pulse-height spectra by an unfolding procedure.[2] Incident charged particles will be rejected by an anticoincidence counter (see Fig. 8.2.2), and gamma rays will be rejected by pulse-shape discrimination. It is hoped that the time width of the proton bursts from the cyclotron will permit pulses produced by high-energy neutrons in the scintillator to be eliminated by time-of-flight. The response of the spectrometer to these high-energy neutrons is not known, and therefore the resulting pulses must be treated as a background. Since this spectrometer will have

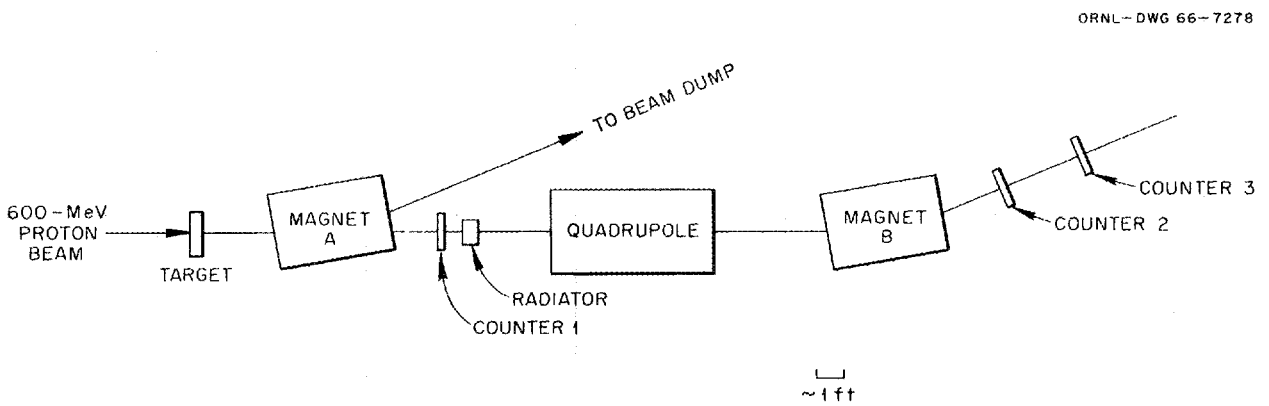

Fig. 8.2.1. Experimental Setup for Measuring Neutron Energy Spectra Above 100 MeV from Targets Bombarded by 600-MeV Protons.

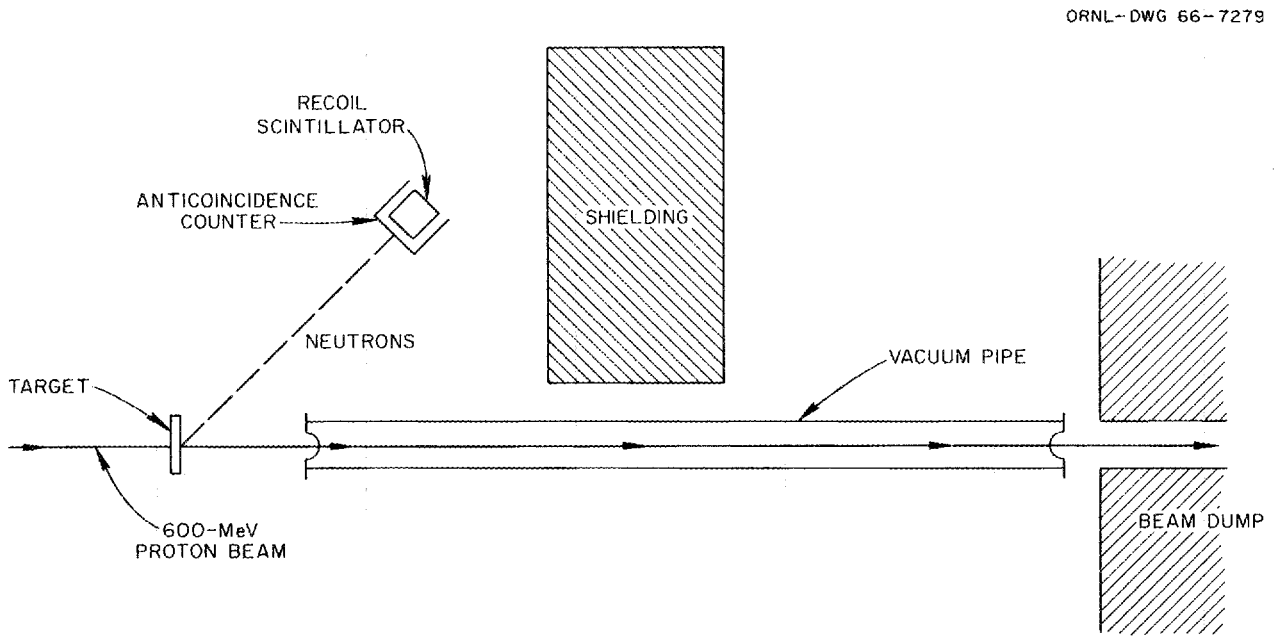

Fig. 8.2.2. Experimental Setup for Measuring Neutron Energy Spectra Between 2 and 50 MeV from Targets Bombarded by 600-MeV Protons.

relatively high efficiency, it is hoped that data may be gathered for a large number of angles and targets.

References

[1]Work partially funded by the National Aeronautics and Space Administration under NASA order R-104(1).

[2]W. R. Burrus and V. V. Verbinski, p. 148 in *Proceedings of the Special Session on Fast Neutron Spectroscopy, Presented at the 1964 Winter Meeting of the American Nuclear Society, San Francisco, Dec. 1, 1964,* Shielding Division Report ANS-SD-2.

8.3 SECONDARY NUCLEON ENERGY SPECTRA FROM TARGETS BOMBARDED BY HIGH-ENERGY PROTONS[1]

J. W. Wachter W. R. Burrus
W. A. Gibson

The analysis of the secondary neutron and proton spectral data obtained with a proton recoil spectrometer (see Sect. 9.7) viewing targets bombarded by 160-MeV protons is nearing completion. These measurements were made on several elements and have been discussed previously.[2,3] Comparisons have been made with the theoretical calculations of Bertini[4] and Kinney.[5] However, several refinements have been made in the experimental data analysis codes, and as a consequence the agreement between theory and experiment has been improved. These refinements included an improvement in the fit between proton energy and corresponding pulse height from the spectrometer and an improvement in the calculated response of the spectrometer to neutrons. The spectra presented here also are a result of combining data obtained for three different thicknesses of recoil proton radiators, whereas the previous data were for one radiator only. Some of the final results are presented in Figs. 8.3.1 and 8.3.2 for neutrons emitted from targets sufficiently thick to stop the primary proton beam. The data were analyzed using the SLOP code,[6] and the spectra have an energy resolution of 25% associated with them. The bands represent the 67% confidence interval. The theoretical results have been adjusted in the following manner to compare with the experimental spectra:

1. The calculated spectra have been smeared with a Gaussian energy distribution to correspond to an energy resolution of 25%.

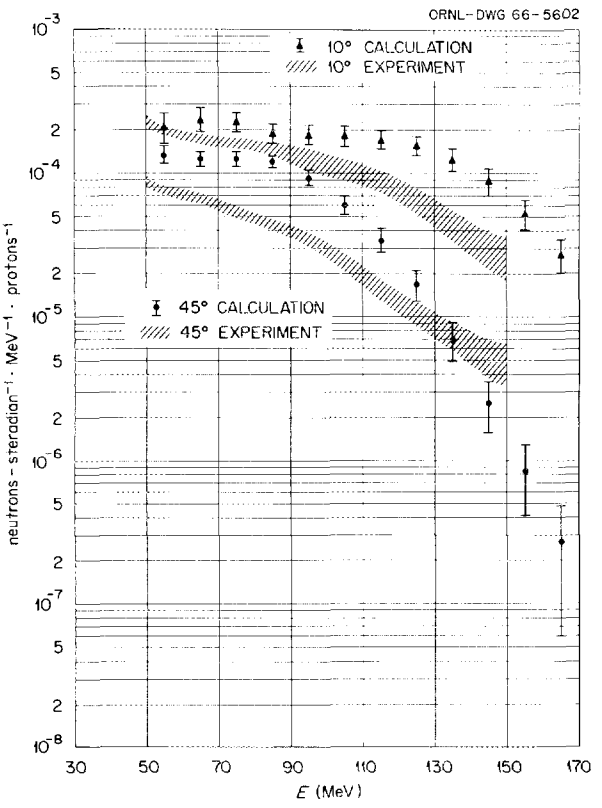

Fig. 8.3.1. Theoretical and Experimental Neutron Spectra at 10 and 45° from 26.89-g/cm^2 Aluminum Target Bombarded by 160-MeV Protons. The theoretical data have been adjusted as outlined in the text.

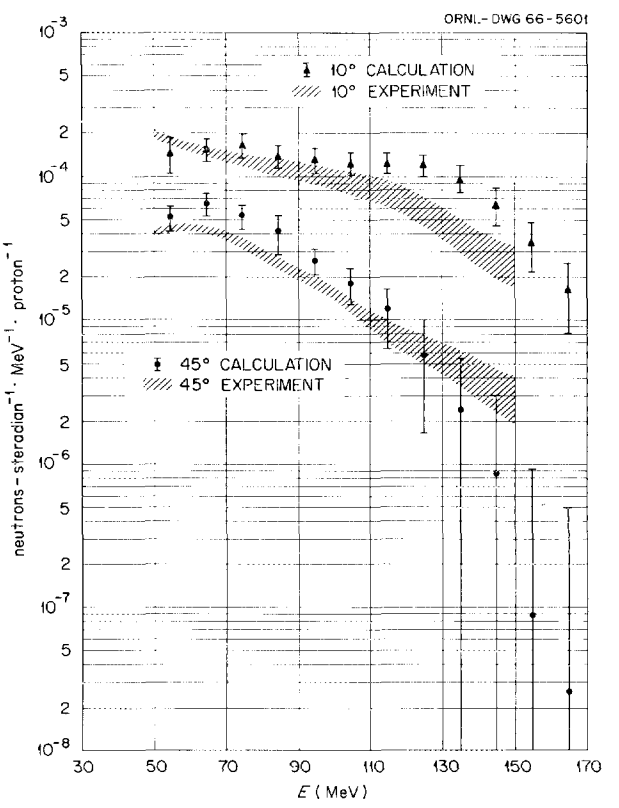

Fig. 8.3.2. Theoretical and Experimental Neutron Spectra at 10 and 45° from 44.33-g/cm^2 Bismuth Target Bombarded by 160-MeV Protons. The theoretical data have been adjusted as outlined in the text.

2. The angular resolution of the calculation was chosen to be 10° so as to be similar to that of the spectrometer.

3. The source was of finite size, and the angular region accepted by the spectrometer varied from point to point. The calculation was modified to include the effect of a finite size source.

In addition to the above experimental spectra, proton data obtained for similar configurations are also being analyzed.

Measurements of the secondary neutron and proton spectra from elements bombarded by 450-MeV protons were reported previously.[7] Considerable improvement has been made in the analysis techniques, and final results are being calculated.

References

[1]Work partially funded by the National Aeronautics and Space Administration under NASA order R-104(1).

[2]W. A. Gibson *et al.*, *Neutron Phys. Div. Ann. Progr. Rept. Aug. 1, 1964,* ORNL-3714, vol. II, p. 124.

[3]W. A. Gibson *et al.*, p. 337 in *Second Symposium on Protection Against Radiations in Space,* NASA SP-71 (1965).

[4]H. W. Bertini, *Monte Carlo Calculations on Intranuclear Cascades,* ORNL-3383 (April 1963).

[5]W. E. Kinney, *The Nucleon Transport Code, NTC,* ORNL-3610 (August 1964).

[6]W. R. Burrus and V. V. Verbinski, p. 148 in *Proceedings of the Special Session on Fast Neutron Spectroscopy, Presented at the 1964 Winter Meeting of the American Nuclear Society, San Francisco, Dec. 1, 1964,* Shielding Division Report ANS-SD-2.

[7]J. W. Wachter, W. R. Burrus, and W. A. Gibson, *Neutron Phys. Div. Ann. Progr. Rept. Aug. 1, 1965,* ORNL-3858, vol. II, p. 88.

8.4 SECONDARY GAMMA RAYS FROM PROTON AND ALPHA BOMBARDMENT OF LIGHT- TO MEDIUM-WEIGHT NUCLEI[1]

W. Zobel
F. C. Maienschein
G. T. Chapman
J. H. Todd[2]

Analysis of the secondary gamma-ray data taken at the Oak Ridge Isochronous Cyclotron with 16-, 33-, and 56-MeV protons and 58-MeV alpha particles on targets ranging in weight from ^{7}Li to Fe has been continued. As was mentioned in the last annual report,[3] some difficulties were encountered in reducing the data obtained with the spectrometer in the total absorption mode, but they have been resolved with the availability of a revised version (FERD) of the original analysis program (SLOP), and reduction of the data is in progress.

For the data taken with the pair spectrometer, the original analysis program continues to give satisfactory results, as it did for the earlier data obtained with 160-MeV protons.[4,5] Reduction of the data for 16- and 33-MeV protons has been completed, and reduction of the data for 56-MeV protons and 58-MeV alpha particles is proceeding smoothly.

Cross sections obtained from the analysis of the pair spectra for the production of various gamma rays in targets of Be, C, O, and Al by incident protons of 16.1 ± 0.2 and 33.1 ± 0.3 MeV are compared with those determined for similar targets bombarded by 160-MeV protons[5] in Tables 8.4.1–8.4.4. In each case the angle of emission of the gamma ray is 135° to the incident proton beam. The proton energies shown in the tables are the average values in the targets, and all results shown have been corrected for self-absorption of the gamma ray in the target.

For beryllium (Table 8.4.1) the most prominent gamma ray that was observed for an incident proton energy of ~160 MeV was that arising from the $^{9}_{4}$Be$(p,\alpha)^{6}_{3}$Li reaction and having an energy of 3560 keV. This gamma ray was also the most intense at the lower proton energies. Gamma rays with energies of 5350 and 5675 keV (not included in the table) were observed for the 160-MeV incident protons, but they were not seen at the lower energies. A weak line at 7700 keV was observed only for the 33-MeV protons.

The results for carbon are shown in Table 8.4.2. As was the case for beryllium, not all the gamma rays were observed at all three incident proton energies. Gamma rays of 2870, 3368, 5031, and 8920 keV were observed at 160 MeV but not at the lower energies.

In the case of oxygen (Table 8.4.3), a 2700-keV line was observed at the two lower energies, but there is no evidence for it at 160 MeV, which is a reversal of the trend observed in the other cases. The targets used for the 160- and 33-MeV runs were

Table 8.4.1. Measured Energies and Cross Sections of Secondary Gamma Rays Produced in a Beryllium Target Bombarded by Protons

Incident Proton Energy (MeV)	Gamma-Ray Energy (keV)	Gamma-Ray Production Cross Section (mb)	Possible Transition	
			Reaction	Energy (keV)
146	3575 ± 15	2.02 ± 0.91	$^{9}_{4}Be(p,\alpha)^{6}_{3}Li$	3560
31	3480 ± 85	3.13 ± 1.81		
14.7	3490 ± 75	6.75 ± 1.91		
146	4390 ± 38	0.72 ± 0.34		
31	4490 ± 95	1.98 ± 1.15		
14.7	4410 ± 85	1.70 ± 0.74		
146	6250 ± 35	0.46 ± 0.22	$^{9}_{4}Be(p,\alpha)^{6}_{3}Li^{*a}$	6190
31	6200 ± 115	2.64 ± 1.21		
14.7	6180 ± 100	1.77 ± 0.62		

[a]Asterisk denotes transition between excited states.

Table 8.4.2. Measured Energies and Cross Sections of Secondary Gamma Rays Produced in a Carbon Target Bombarded by Protons

Incident Proton Energy (MeV)	Gamma-Ray Energy (keV)	Gamma-Ray Production Cross Section (mb)	Possible Transition	
			Reaction	Energy (keV)
145	2014 ± 40	5.44 ± 1.99	$^{12}_{6}C(p,pn)^{11}_{6}C$	1990
30.3	1950 ± 70	12.50 ± 8.6		
145	4480 ± 50	11.40 ± 4.1	$^{12}_{6}C(p,p')^{12}_{6}C$ and/or $^{12}_{6}C(p,2p)^{11}_{5}B$	4433
30.3	4370 ± 95	91.50 ± 11.1		
14.6	4340 ± 140	265.00 ± 21.0		4460
145	6750[a]	3.03 ± 1.09		
30.3	6650	23.6 ± 3.7		

[a]Average energy for several gamma rays, not resolved.

Table 8.4.3. Measured Energies and Cross Sections of Secondary Gamma Rays Produced in an Oxygen Target Bombarded by Protons

Incident Proton Energy (MeV)	Gamma-Ray Energy (keV)	Gamma-Ray Production Cross Section (mb)	Possible Transition	
			Reaction	Energy (keV)
145	2320 ± 25	6.7 ± 3.0	${}^{16}_{8}O(p,2pn){}^{14}_{7}N$	2311
28.2	2250 ± 70	7.6 ± 5.6		
28.2	2700 ± 75	3.7 ± 3.6	${}^{16}_{8}O(p,p'){}^{16}_{8}O^{*a}$	2740
12.1	2700 ± 70	16.2 ± 7.3		
145	4430 ± 30	15.8 ± 5.7	${}^{16}_{8}O(p,p\alpha){}^{12}_{6}C$	4433
28.2	4340 ± 95	83.4 ± 13.2		
145	5260 ± 25	12.0 ± 4.9	${}^{16}_{8}O(p,pn){}^{15}_{8}O$ and/or	5240
28.2	5200 ± 105	51.2 ± 8.0	${}^{16}_{8}O(p,2p){}^{15}_{7}N$	5276
145	6290 ± 35	55.6 ± 19.7	${}^{16}_{8}O(p,p'){}^{16}_{8}O$	6140
28.2	6100 ± 115	101.0 ± 14		
12.1	6170 ± 100	79.6 ± 11.1		
145	7100 ± 50	12.3 ± 4.4	${}^{16}_{8}O(p,p'){}^{16}_{8}O$	7120
28.2	6960 ± 125	40.8 ± 5.8		
12.1	7050 ± 100	46.6 ± 6.9		

[a]Asterisk denotes transition between excited states.

Table 8.4.4. Measured Energies and Cross Sections of Secondary Gamma Rays Produced in an Aluminum Target Bombarded by Protons

Incident Proton Energy (MeV)	Gamma-Ray Energy (keV)	Gamma-Ray Production Cross Section (mb)	Possible Transition	
			Reaction	Energy (keV)
145	2250 ± 25	7.3 ± 9.2	${}^{27}_{13}Al(p,p'){}^{27}_{13}Al$	2219
30.0	2200 ± 70	49.7 ± 33.4		
14.4	2200 ± 65	152.0 ± 33.0		
145	2770 ± 50	10.7 ± 8.4	${}^{27}_{13}Al(p,\alpha){}^{24}_{12}Mg^{*a}$	2753
14.4	2750 ± 70	14.3 ± 12.1		
30.0	2950 ± 80	17.0 ± 19		
14.4	2980 ± 70	88.0 ± 23		
145	3400 ± 20	2.2 ± 5.1	${}^{27}_{13}Al(p,2pn){}^{25}_{12}Mg$	3410
30.0	3380 ± 85	6.0 ± 11		

[a]Asterisk denotes transition between excited states.

water, but a BeO target was used for the 16-MeV run because of mechanical problems associated with preparing a sufficiently thin water target. The contribution due to the beryllium was subtracted from the results.

As was noted in the report on the 160-MeV data,[5] aluminum was the lightest target in which a continuum was observed to underlie the discrete line structure. The cross sections quoted in Table 8.4.4 for the various lines have been corrected by subtracting this continuum. No gamma rays with energies greater than 3410 keV were observed for 33- and 16-MeV incident protons.

References

[1]Work funded by the National Aeronautics and Space Administration under NASA order R-104(1).

[2]Instrumentation and Controls Division.

[3]G. T. Chapman *et al.*, *Neutron Phys. Div. Ann. Progr. Rept. Aug. 1, 1965*, ORNL-3858, vol. II, pp. 82–85.

[4]W. Zobel, F. C. Maienschein, and R. J. Scroggs, *Neutron Phys. Div. Ann. Progr. Rept. Aug. 1, 1964*, ORNL-3714, vol. II, p. 120.

[5]W. Zobel, F. C. Maienschein, and R. J. Scroggs, *Spectra of Gamma Rays Produced by the Interaction of ~160-MeV Protons with Be, C, O, Al, Co, and Bi*, ORNL-3506 (April 1965).

8.5 BEAM ENERGY MEASUREMENTS AT THE OAK RIDGE ISOCHRONOUS CYCLOTRON[1]

R. T. Santoro — T. A. Love
F. E. Bertrand[2] — R. W. Peelle

Measurements have been made of the beam energy of the Oak Ridge Isochronous Cyclotron for protons at acceleration frequencies of 17.04 and 21.22 Mc, H_2^+ ions at 11.32, 11.91, and 12.61 Mc, and alpha particles at 11.32 Mc. The energy was determined from measurements of the particle pathlength in aluminum using a remotely controlled range wheel to vary the absorber thickness. Experimental results are given in tabular form. A curve of measured proton energy as a function of rf acceleration frequency is included.

References

[1]Abstract of ORNL-TM-1382 (Jan. 13, 1966); work funded by National Aeronautics and Space Administration under order R-104(1).

[2]Oak Ridge Graduate Fellow from Louisiana State University under appointment from the Oak Ridge Associated Universities.

8.6 EVALUATION OF QUIKTRAN REAL TIME COMPUTER TERMINAL[1]

W. R. Burrus

Within the next few years, individual desk-top computer input/output terminals are expected to become widely available at a price competitive with conventional desk calculators. Looking ahead to the time when such facilities could be made available through a local centralized computer center, we acquired a commercially available real time computer terminal (IBM's QUIKTRAN) in June of 1965. We wanted to evaluate its effectiveness on typical Division problems and to make it available to all interested persons to develop an awareness of its limitations and potentialities.

The operational characteristics of our QUIKTRAN terminal are summarized below:

Input:	Typewriter keyboard at typing speed IBM cards at about 10 cards/min Punched paper tape at about 5 characters/sec
Output:	Typewriter printer at about 5 lines/min IBM cards at about 10 cards/min
Language:	QUIKTRAN – a subset of FORTRAN. Its major inconsistency is that arrays are not permitted as subroutine arguments; compiling is done one line at a time, which allows powerful debugging and error correction to be done during execution
Speed:	Approximately ten arithmetic operations per second
Storage Capability:	Approximately 50 modest-size programs or approximately 60,000 words of data

The terminal, which is now available for 4 hr during the afternoon, was initially used about 30 hr per month and is now being used about 45 hr per month. The terminal is used on an informal (signed for in advance) basis and is seldom signed for more than one or two days in advance.

One of the important results of our evaluation is that we now have a realistic idea of the extent of interest in remote terminals. At installation, personnel from our division, from both computing centers, and from other divisions were invited to use the terminals for evaluation on their problems. To date, about 26 persons have used the terminal for an hour or more: 10 from our own division, 15 from other divisions, and one from a computing center. Encouraged by these evaluations, three other groups have initiated proceedings to obtain similar service.

The problems which have been run were usually of the following types:

1. *Problems which would ordinarily be run on a desk calculator and require 4 to 8 hr of time.* – These are usually not sent to one of the computer centers because of the several days of delay in getting a program debugged and run. Such programs were typically debugged and run on QUIKTRAN in less than an hour. Approximately 20% of the time has been used for such jobs.

2. *Applications which require quick answers in order to evaluate the progress of an experiment.* – Several potential applications have been programmed for QUIKTRAN, but its speed is too slow by a factor of at least 10 for many applications. Also, the paper-tape reading equipment is very inflexible and could not accept any of our standard formats.

3. *Debugging of FORTRAN programs which were to be run later at one of our computer centers.* – It has become common practice for a program that is needed in a hurry to be tested on QUIKTRAN before submission. QUIKTRAN is also useful for leisurely debugging of longer programs, but the program restrictions proved to be awkward. It became especially clear from the experience of our novice programmers that QUIKTRAN is a very effective teacher. Approximately 70% of the time has been used in this way.

4. *Retrieval of frequently used information.* – Programs were incorporated into the system for providing gamma-ray cross-section data (from G. W. Grodstein's data by interpolation), for neutron cross sections, and charged-particle stopping power. The gamma-ray cross-section program was seldom used, however, because looking up the information in Grodstein (and interpolating it graphically) proved to require less time than the 1 or 2 hr waiting time required to obtain a QUIKTRAN terminal. Some success was obtained with charged-particle stopping powers (which are not quite so easy to look up in a report), but the neutron cross section proved to be intractable because of the limited storage ability of QUIKTRAN.

Some programs that are presently in the system storage are the following:

1. Range and dE/dx for protons in various materials (from Bethe Block formula with empirical shell corrections).
2. Pulse-height data manipulation from standard BSF card format.
3. Demonstration information retrieval program which retrieves titles from a list of 30 papers by multiple keywords (Metals and Ceramics Division).
4. Programs for plotting results on printer.
5. Least-squares routine which will accommodate up to 20 variables and 1000 knowns (executes concurrently with input).
6. Gamma-ray spectrum unfolding code (200-channel spectrum in about 20 min).
7. Critical-path (PERT) program (supplied by IBM).
8. Coordinate geometry for engineering problems (supplied by IBM).
9. Conversational matrix manipulation language program (supplied by IBM).
10. Solid-angle acceptance factors for disk and cylinder sources.

In addition, there are approximately 40 debugged QUIKTRAN programs to interpolate, integrate, etc., which are available at the console on card decks for combining into larger programs.

Our evaluation has been successful enough so that we can now see the next logical step. It

appears that we should seek a more advanced system for further evaluation with the following characteristics:

1. The terminals should be sufficiently inexpensive that they can be located wherever needed, in the same manner that desk calculators are utilized. This puts about a $50/month ceiling on the hardware cost of adding an additional terminal to the system.
2. The language should be upward and downward compatible with one of the standard languages available at our computer centers.
3. The arithmetic speed should be at least 100 operations/sec.
4. The system should be open-ended, and should allow machine language routines to be entered by the user from his console.
5. An optional graphic feature (for displaying curves of experimental data, etc.) comparable in cost to the basic terminal should be made available.
6. Each user should have about 10^6 words of storage available to him for programs and data.
7. The terminals should be portable; that is, they should be capable of being disconnected like an extension telephone, and moved from one experiment or office to another.

From the operational experience with QUIKTRAN, we can postulate that the present demand is for about 16 terminals within the Neutron Physics Division, and perhaps 20 within other divisions and the computer centers. In our division, we anticipate that the individual terminals would be used from a few minutes per day to perhaps 4 hr, with the average being about $1\frac{1}{2}$ hr per day per terminal.

There are many questions concerning the potential efficiency or inefficiency of computer terminals, and they can be answered only by experimenting with the terminals in the context of the special problems involved. Some advantage might result from extending the experimentation to a larger group of persons, but a larger group cannot move as fast or with as great flexibility as a smaller group. The deciding factor is whether there is sufficient interest outside the division to lead to some initiative.

There appears to be no technical, economic, or equipment constraint that would prevent us from obtaining a system with all the characteristics desired by the end of the year. It is expected that any hardware obtained would be either leased or purchased. In the latter case, it must be compatible with subsequent local developments.

References

[1]Work funded by the National Aeronautics and Space Administration under NASA order R-104(1).

8.7 MEASUREMENTS OF (p,n) NEUTRON-PRODUCTION CROSS SECTIONS FOR 18.5- AND 15.1-MeV PROTONS ON Be, N, Al, Fe, In, Ta, AND Pb AT ANGLES OF 0 TO 170° AND NEUTRON ENERGIES ABOVE 0.8 MeV[1]

V. V. Verbinski W. R. Burrus
M. Young[2]

Measurement of (p,n) interactions for a number of target materials was initiated last year in order to provide direct shielding data for spacecraft passing through the Van Allen belt and, more generally, to test neutron-production calculations at lower proton bombarding energies, where the accuracy of the calculations has not been determined. Cross-section measurements for neutrons emitted at up to seven angles between 0 and 170° were obtained for neutrons above 0.8 MeV from 18.5- and 15.1-MeV protons on Be, N, Al, Fe, In, Ta, and Pb. These neutron measurements were made with a proton-recoil scintillation spectrometer which used a 2-in.-diam by 2-in.-high liquid organic scintillator and an unfolding technique which converts pulse-height spectra to absolute neutron spectral intensity. A number of difficulties have recently been cleared up, and the spectrometer has satisfactorily passed a series of tests, some of which are described in Sect. 6.4.

One of the difficulties with the spectrometer related to the nonreproducibility of results when either the photomultiplier tube base or (even) the photomultiplier tube was changed. This difficulty was traced to pickup at dynode 10 of the much larger signals existing at dynode 14 and anode. The latter signals intentionally show a saturation

effect for optimum operation of the gamma-rejection pulse-shape discriminator. This difficulty was cleared up eventually by taking the linear signal from dynode 11, improving the grounding arrangement, shielding the linear signal from the higher dynodes, and moving the pulse-shape discriminator circuitry closer to the ground plane. Three different tube base constructions with the above improvements included were then found to provide results that were satisfactorily reproducible.

Unfortunately, the (p,n) measurements had been made with an unsatisfactory tube base. But fortunately, a Po-Be pulse-height distribution was measured with the old base at the time that the (p,n) measurements were made. Comparison of that pulse-height distribution with one obtained with a clean base provided a small but significant correction to the earlier pulse-height distributions, a correction for the nonlinearity produced by pickup signals. A simple correction code was written and has been applied to the (p,n) data, and the neutron energy spectra and cross sections are being computed from the raw data at the time of this writing.

References

[1]Work funded by the National Aeronautics and Space Administration under NASA order R-104(1).

[2]Mechanical and Aerospace Department at Louisiana State University, Baton Rouge, La.

8.8 ^{9}Be(α,n) NEUTRON-PRODUCTION CROSS SECTIONS vs NEUTRON ENERGY AND ANGLE FOR 6- TO 10.5-MeV ALPHA PARTICLES[1]

V. V. Verbinski W. E. Kinney
J. K. Dickens F. G. Perey

Measurements of the ^{9}Be$(\alpha,n)^{12}$C cross sections for alpha particles between 6 and 10.5 MeV were reported in part previously.[2] Hand-processed data for 0° cross sections and excitation functions were shown. This was done for the (α,n_0) or ground-state neutrons, and also for the (α,n_1) neutrons, because these neutrons were well separated in energy from each other and from other neutrons, and gave rise to two distinct plateaus in the pulse-height distribution at the highest pulse heights. Some preliminary results unfolded with the FERDO code developed by Burrus showed that the (α,n_2) neutrons could easily be unravelled. Since this type of spectrometry had not until recently passed a number of stringent tests, the FERDO code could not be used with confidence to process the earlier data. Some of these difficulties are discussed in Sect. 8.7 and also in Sect. 6.4. The data are being processed at the time of this writing, and the double differential cross section at alpha-particle bombarding energies of 6 to 10.5 MeV should soon be completed. These cross sections will be angle- and energy-integrated (above about 0.8 MeV) and compared with those obtained by Gibbons and Macklin,[3] who used a 4π graphite-moderated long counter. A preliminary comparison of their results with ours indicated that an abundance of low-energy neutrons is given off at higher alpha-particle energies, possibly leading to three- or four-body breakup [i.e., $^9\mathrm{Be}(\alpha,n\alpha')^8\mathrm{Be} \rightarrow n + 3\alpha$].

References

[1]Work funded by the National Aeronautics and Space Administration under NASA order R-104(1).

[2]V. V. Verbinski *et al.*, *Neutron Phys. Div. Ann. Progr. Rept. Aug. 1, 1964*, ORNL-3714, vol. II, p. 131.

[3]J. H. Gibbons and R. L. Macklin, *Phys. Rev.* **114**, 571 (1959); R. L. Macklin, *Nucl. Phys.* **1**, 335 (1963).

9. Radiation Detector Studies (II)

9.1 MULTIPLE COULOMB SCATTERING INTO A DETECTOR IN CHARGED-PARTICLE COINCIDENCE MEASUREMENTS BETWEEN REACTION PRODUCTS[1]

R. W. Peelle

Assuming that the particles which strike a circular detector have been displaced by multiple Coulomb scattering according to a bivariate normal density function, this note displays the fraction of the detected particles which if undeflected would have struck the detector plane outside a circle of specified larger radius. The problem is solved exactly by numerical quadrature and is solved approximately if the rms displacement caused by the scattering is much less than the detector radius. The latter form may be employed for noncircular detectors. Numerical results are compared for a wide range of cases.

The results of this calculation are applicable to experiments in which the output particles from a binary reaction are observed in coincidence. Multiple scattering in the target or in an interposed material causes some of the charged particles striking the first detector to have conjugate particles outside the kinematically prescribed cone which maps the first detector in the plane of the second, and so the second detector must be larger than would be estimated with multiple scattering ignored. This correction is important to scintillator neutron efficiency measurements by the $D(T,{}^4He)n$ reaction, and should apply to other experiments where coincidence detection is used to define the reaction being studied. The results are tentative in that the normal density function is not a very accurate description of the multiple scattering.

References

[1]Abstract of ORNL-TM-1517 (in press); work funded by the National Aeronautics and Space Administration under NASA order R-104(1).

9.2 A TOTAL-ABSORPTION DETECTOR FOR 60-MeV PROTONS USING LITHIUM-DRIFTED GERMANIUM[1]

F. E. Bertrand[2] R. J. Fox[3]
R. W. Peelle N. W. Hill[3]
T. A. Love H. A. Todd[3]

A lithium-drifted germanium diode has been used for total-absorption detection of 59-MeV protons from the Oak Ridge Isochronous Cyclotron. The detector is 1.9 cm in diameter, has a depletion depth of 6 mm, is cooled to less than 85°K, and is sealed in an aluminum can with a 0.0026-in.-thick window. The diode was oriented so that the protons entered in a direction parallel to the detector junction.

The energy resolution attained for 59-MeV protons was 150 keV (FWHM), uncorrected for energy straggling in windows of 76 keV, for approximately 60 keV of beam resolution, and for electronic noise. The peak-to-total ratio, determined by using an anticoincidence collimator, was as high as 0.94, which is comparable with 0.96 observed elsewhere[4] for NaI. When the collimator was moved along a line parallel to the junction and perpendicular to the beam, the energy resolution and peak-to-total ratios remained constant within the experimental accuracy over a 10-mm scanned distance. As the collimator was moved in a direction perpendicular

to the junction and toward the depleted material, the peak-to-total ratio decreased, as was expected from multiple-scattering calculations.

When the diode was connected by a 125-Ω terminated coaxial cable to a fast amplifier, a rise time of 4 to 5 nsec was observed. Since the protons entered the detector parallel to the junction, pictures obtained show the superposition of nearly rectangular current pulses arising from hole and electron collection. The length of the pulses is correlated with the point of incidence of the collimated beam. The mobilities of the charge carriers as calculated from the measured collection times and a knowledge of the location of proton incidence are 13,000 $cm^2/Vsec$ for the electrons and 9800 $cm^2/Vsec$ for holes for a detector bias of 500 V. With detector biases of 200 and 700 V, the mobilities are 60% higher and 30% lower respectively.

References

[1]Abstract of ORNL-TM-1462 (March 1966); work funded by the National Aeronautics and Space Administration under NASA order R-104(1).

[2]Oak Ridge Graduate Fellow from Louisiana State University under appointment from the Oak Ridge Associated Universities, Inc.

[3]Instrumentation and Controls Division.

[4]D. F. Measday, *Nucl. Instr. Methods* **34**, 353 (1964).

9.3 TEMPERATURE DEPENDENCE OF THE RESPONSE OF LITHIUM-DRIFTED GERMANIUM DETECTORS TO GAMMA RAYS[1]

M. M. El-Shishini[2] W. Zobel

While it has generally been stated that lithium-drifted germanium detectors must be operated at liquid-nitrogen temperature for optimum performance, no systematic investigation to prove or disprove this statement has been reported. The closest experiment is that of Tavendale,[3] who, however, investigated the resolution as a function of temperature for only one low-energy gamma ray.

We have investigated the resolution and efficiency of two lithium-drifted germanium detectors, approximately 20 mm in diameter and 3 mm thick, as a function of detector temperature in the range 85 to 160°K. Gamma-ray energies ranged from 279 keV (^{203}He) to 1333 keV (^{60}Co). We found that, contrary to the results of Tavendale, the resolution of the detectors had a pronounced peak at about 105°K. The origin of this peak is at present unknown, but is not due to changes in diode capacitance or leakage current. The efficiency of the diodes is approximately constant for each energy over the temperature range.

Since both detectors were cut from the same germanium ingot, it is possible that these results are peculiar to these detectors. It is therefore proposed to repeat the experiment with a detector produced from a different germanium ingot, as soon as such a detector becomes available.

References

[1]Abstract of ORNL-TM-1295 (in press); also to be published in the *Proceedings of the 10th Scintillation and Semiconductor Symposium.* Work partially funded by the National Aeronautics and Space Administration under NASA order R-104(1).

[2]United Arab Republic.

[3]A. J. Tavendale, *Inst. Elec. Electron. Engrs., Trans. Nucl. Sci.* **NS-11**, 191 (1964).

9.4 SIMULTANEOUS CONNECTION OF FAST- AND SLOW-AMPLIFIER SYSTEMS TO SEMICONDUCTOR SYSTEMS[1]

N. W. Hill[2] R. W. Peelle

Experiment designs often require the time information contained in the signals from semiconductor detectors as well as the customary information on the amount of deposited energy. For example, the timing information is important to scintillator calibration using semiconductor detection of helium recoils in coincidence with neutrons from the $T(d,n)^4He$ or $D(d,n)^3He$ reactions,[3] and both types of information are needed for charged-particle identification and spectrometry in current studies of secondary charged particles from 60-MeV incident protons.[4]

Measurements of deposited energy in semiconductors usually depend on observation of the total charge release by the event, using charge-sensitive

preamplifiers designed for stability and low noise rather than for rapid response. Since the time interval required for full collection of the charge carriers depends on the position of an event in the detector, the least ambiguous timing information lies in the first movement of charge carriers in the semiconductor. Sensing this first voltage change across the diode requires amplifiers and signal connections which allow fast transient response with minimum noise, although stability need not be perfect.

We have attempted to determine which amplifier and signal connection configurations give good overall performance for the various types of semiconductor detectors in use. Most of our work has been concerned with either thin (about 200-μ, 100-pF) totally depleted silicon surface-barrier diodes or thick (6-mm, 20-pF) lithium-drifted germanium diodes. The criteria for system design have been clean fast signals with minimum noise for the signal rise time, slow amplifier resolution and stability essentially unhampered by the presence of the fast system, and the ability to operate at least some of the amplifiers at a distance from the detector, which often seems to be required by the geometry of accelerator experiments.

The two types of detectors considered represent interesting extreme cases with respect to the signals produced at the detector. A 200-μ silicon detector, particularly if chilled to dry-ice temperature, has an electron collection time as short as 1 nsec, shorter than the corresponding discharge time of the ~40-pF diode into a 50-Ω coaxial cable and comparable with the available rise times from existing fast transistor amplifiers with a gain of 10^3 or greater. The germanium detector, on the other hand, has collection times in the neighborhood of 100 nsec for a 6-mm compensated region; so the rise time of the resulting pulse depends directly upon the impedance of the discharge path. A rise time of about 5 nsec has been observed[5] using a terminated 125-Ω system with no slow amplifier connection.

No satisfactory approach for good time and energy resolution is readily apparent without a fast and a slow amplifier channel. Though other design choices are possible,[6–9] we have employed charge amplifier circuits derived from conventional design,[10] current-mode fast amplifiers with low input impedance,[11–13] and connection schemes in which each amplifier is connected to the diode without intervening active elements. Within this framework we have considered the effects of each amplifier on the signal-to-noise ratio of the other and the effects on the fast signal shape and amplitude of reflections along coaxial lines connecting the detector to either amplifier, of the feedback signal from the output of the charge-sensitive slow amplifier, and of the resonant circuit consisting of the diode capacity and the connecting lead inductance damped by the fast-amplifier input impedance.

Figure 9.4.1 illustrates a fairly successful arrangement for thin silicon detectors, assuming that both sides of the mount are accessible and that the slow amplifier (which cannot terminate any cable) can be mounted very close to the detector. The transformer coupling to the fast amplifier, which has an input impedance of about 10 Ω, is arranged to provide proper damping of the series resonant circuit of the diode and its connections, to give the maximum current into the fast amplifier, and to reduce noise fed into the slow system. If a cable connects the slow amplifier to the diode, the ratio of primary to secondary transformer turns must be chosen to match this cable impedance for the fast rise time portion of the pulse. Minimum rise times were observed when the transformer could be omitted. The fast signal in Fig. 9.4.1 appears across the slow amplifier input capacity and the stray capacity, C_s, in series with the diode capacity; so the fast signal can be augmented by

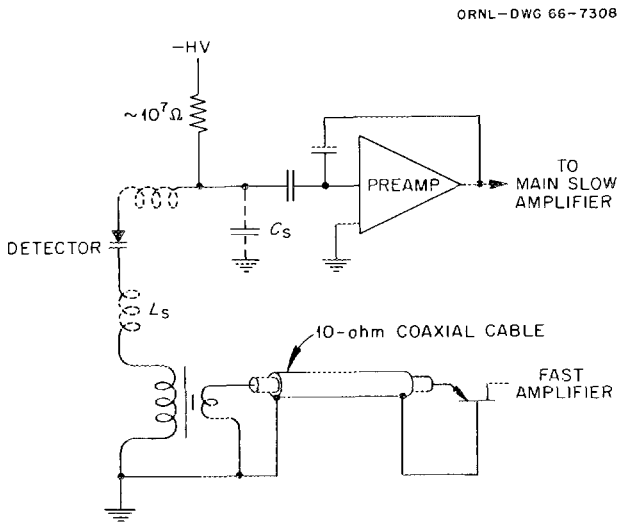

Fig. 9.4.1. Typical Connection Employed for a Thin Silicon Diode.

increasing C_s until the energy resolution seen by the slow system is compromised. A more desirable way to accomplish this is to use parallel field-effect transistors at the slow-amplifier input. This greatly increases the effective capacity without appreciably increasing the noise in the slow amplifier. Though we have referred to the charge amplifier as slow, the system benefits from having fast response so that the fedback charge does not unduly lengthen the pulse seen in the fast amplifier. Using a room-temperature, 40-μ, 100-pF diode in an arrangement such as that shown in Fig. 9.4.1 but with no transformer, clean fast signals (2.2 nsec rise time, 3.5 nsec wide) were obtained without measurable broadening of the slow-amplifier resolution.

In the case of lithium-drifted germanium detectors, only one side of the diode is readily available for signal connection, and some lead length is required because the detector must rest in a cryostat at liquid-nitrogen temperature. The most successful dual connection seems to involve transformer coupling located adjacent to the slow-amplifier input as in Fig. 9.4.2 with parallel field effect input transistors on the slow amplifier to increase its effective input capacity. If the cable between pickoff transformer and slow preamplifier is made very short in the system of Williams and Biggerstaff,[14] their system is similar to the one described here except that the fast amplifier and the coupling transformers are of different types. A fast threshold below 200 keV and above noise has been reached with a fast-amplifier rise time of 12 nsec, over twice that allowed by the detector.

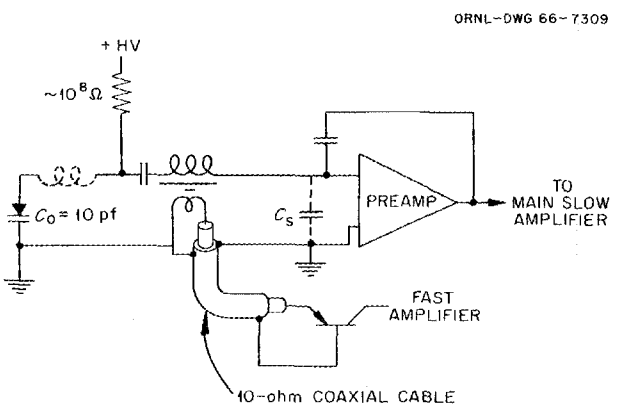

Fig. 9.4.2. Typical Connection for Lithium-Drifted Germanium Detector.

The slow preamplifier, cut for proper operation with random 60-MeV input, has a gamma-ray resolution of about 13 keV, not definitely changed by turning on the fast amplifier. Thus the effect of the fast amplifier was to introduce a noise component to less than 5 keV, plus the effect of the stray transformer capacity. On the other hand, the slow preamplifier made an important noise contribution to the fast system via high-frequency noise components from the field-effect transistor.

In all cases fast signal performance can be improved if no slow signal is required or if experiment requirements permit the slow amplifier's energy resolution to be degraded appreciably. Of the criteria set above, the most difficult criterion has been the remote location from the detector of the slow amplifier, although the systems are degraded only slightly by remote location of the fast amplifiers.

References

[1]Work funded by the National Aeronautics and Space Administration under NASA order R-104(1).

[2]Instrumentation and Controls Division.

[3]T. A. Love *et al.*, *Absolute Efficiency Measurements of NE-213 Organic Phosphors for the Detection of Neutrons at Energies of 14.4 and 2.6 MeV*, ORNL-3893 (in press).

[4]F. E. Bertrand *et al.*, *Neutron Phys. Div. Ann. Progr. Rept. Aug. 1, 1965*, ORNL-3858, vol. II, p. 85; see also sect. 8.1 of this report.

[5]F. E. Bertrand *et al.*, *A Total-Absorption Detector for 60-MeV Protons Using Lithium-Drifted Germanium*, ORNL-TM-1462 (in press).

[6]H. Wahl, *Nucl. Instr. Methods* **25**, 247 (1964).

[7]M. A. Basire, B. deCosnac, and J. Labbee, French Commissariat a l'Energie Atomique (private communication 1963).

[8]A. Alberigi *et al.*, "Experimental Results on the Information Available from the Rise Time of Pulse Supplied by Semiconductor Particle Detectors," Instituto Nazionale di Fisica Nucleare, INFN/TC-65/13.

[9]T. K. Alexander and G. C. Neilson, "Electronic Timing with a Solid-State Detector," APS, Edmonton Meeting, August 1963.

[10]T. V. Blalock, *Optimization of Semiconductor Preamplifier for Use With Semiconductor Radiation Detectors*, ORNL-TM-1055 (1965).

[11]E. J. Kennedy, Oak Ridge National Laboratory (private communication 1966).

[12]J. K. Millard, Oak Ridge National Laboratory (private communication 1966).

[13]C. J. Rush, *Rev. Sci. Instr.* **35**, 149 (1964).

[14]C. W. Williams and J. Biggerstaff, *Nucl. Instr. Methods* **25**, 370 (1964).

9.5 RESPONSE FUNCTION FOR NEUTRON TIME-OF-FLIGHT SPECTROSCOPY[1]

R. T. Santoro R. W. Peelle

Experiments have been performed using time-of-flight techniques to measure the differential cross sections for the production of neutrons resulting from the interactions of 160-MeV protons with target nuclei.[2] As part of the analysis of these data, a study has been started to determine the time response function for monoenergetic neutrons in the experimental geometry.

Figure 9.5.1 shows the arrangement of the target and detector in a typical experimental configuration. A cartesian coordinate system, xyz, is constructed such that the x axis is along the direction of the beam. The xy plane contains the center of the detector and the target normal. The target position is described by a rotation angle, Ψ, between the beam axis and the target normal, $\hat{\xi}$. The target coordinate system ξ-η is constructed so that the vertex of the ξ-η system is in conjunction with the origin of xyz, with ξ and η constrained to rotate in the xy plane. The target thickness T is measured along ξ such that $\tau_2 - \tau_1 = T$ and

$$\tau_1 \leq \xi \leq \tau_2 \tag{1}$$

for all values of ξ in the target. The position of the neutron detector is given by θ and $|\vec{L}|$, where $\vec{L}$ is a vector in the xy plane from $x = y = z = 0$ to the face of the detector and normal to it, and θ is the angle between the x axis and $\vec{L}$.

Protons incident on the target parallel to the x axis interact in an element of target volume $dx\ dy\ dz$, producing secondary neutrons of velocity v_n. The flight times of neutrons which are born in the target and interact in the detector are measured. The apparent flight time t is given by

$$t = t_p + t_n + t_c\ , \tag{2}$$

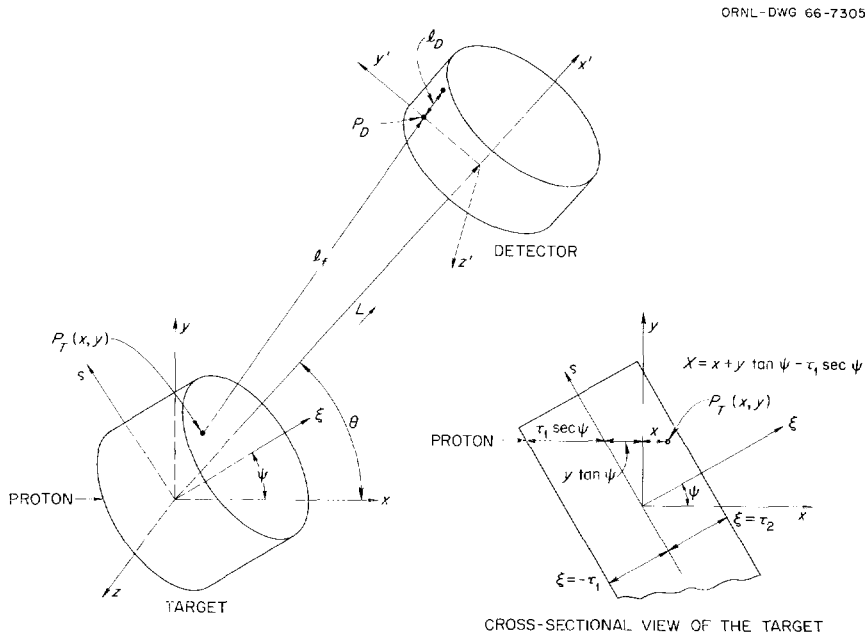

Fig. 9.5.1. Schematic Arrangement of the Target and Detector for the Measurement of the Flight Times of Secondary Nucleons.

where t_p is the interval between the passage of the proton past an arbitrary zero-time reference point and the time of interaction in the target, t_n is the flight time of the neutron between its birth and detection, and t_c is the time required for light to travel through the detector from the point of interaction to the photocathode of the multiplier tube. It is assumed that phototube delays are independent of the position at which the light strikes the photocathode.

The probability per MeV of neutron energy that a neutron of speed v_n has an apparent flight time within dt at t is given by

$$C(t,v_n)\ dt = dt \iiint N(y,z)\ B(X,\vec{\Omega}) \times E_{\oplus}(t,X,x,v_n)\ dx\ dy\ dz\ . \quad (3)$$

$B(X,\vec{\Omega})\ dx$ is the probability per unit solid angle per MeV of neutron energy that the proton interacts in the target within dx at a penetration $X = x + y \tan \Psi - \tau_1 \sec \Psi$ to produce a neutron which is emitted in the direction Ω:

$$B(X,\vec{\Omega})\ dx \begin{cases} = \Sigma_p(v_p;v_n,\vec{\Omega}) \exp(-\Sigma_{TP}^{\text{eff}}\ X)\ dx & \text{for } x,y \text{ within the target ,} \\ = 0 & \text{for } x,y \text{ outside the target ,} \end{cases} \quad (4)$$

where

$\Sigma_p(v_p;v_n,\vec{\Omega})$ = the differential cross section per MeV per unit solid angle in the direction $\vec{\Omega}$ for the production of neutrons of speed v_n,

Σ_{TP}^{eff} = the effective cross section for absorption of protons in the target.

Since the direction of emission of the neutron is taken to be independent of the azimuthal angle, $\Sigma_p(v_p;v_n,\vec{\Omega})$ reduces to $\Sigma_p(v_p;v_n,\oplus)$, where $\oplus$ is the angle of neutron emission relative to the beam axis.

$N(y,z)\ dy\ dz$ is the probability that a beam particle has a displacement from the beam axis within dy at y and within dz at z; $N(y,z)$ is approximated in this analysis by a bivariate normal frequency function. From previous calculations[3] it has been shown that the z component of the beam introduces negligible flight-path variations. Based on these results, $E_{\oplus}(t,X,x,v_n)$ is considered to be independent of z, and, since $N(y,z)$ is the only term in which z is contained explicitly, it is integrated immediately over all values of z with the result that

$$dy \int N(y,z)\ dz = N(y)\ dy\ . \quad (5)$$

$E_{\oplus}(t,X,x,v_n)\ dt$ is the probability that a neutron of velocity v_n born at x,y in the target and emitted in a unit solid angle toward the detector is detected within dt at t:

$$E_{\oplus}(t,X,x,v_n)\ dt = \iint_{\substack{\text{detector}\\ \text{face}}} I(t,X,x,v_n,\vec{\Omega})\ d\vec{\Omega}\ dt\ , \quad (6)$$

where

$$I(t,X,x,v_n,\vec{\Omega}) \begin{cases} = \exp(-\Sigma_{TN}^{\text{eff}}\ l_T)\ \Sigma(v_n)\ v_n \exp[-\Sigma_D^{\text{eff}}\ l_D(t)] & \text{for } l_D(t) \text{ in the detector ,} \\ = 0 & \text{for } l_D(t) \text{ outside the detector ,} \end{cases} \quad (7)$$

in which

Σ_{TN}^{eff} = effective macroscopic absorption cross section for neutrons in the target,

$\Sigma(v_n)$ = macroscopic "efficiency" cross section for neutron detection,

Σ_D^{eff} = effective macroscopic absorption cross section for neutrons in the detector,
v_n = neutron energy,
l_T = path length traveled by the neutron in the target,
$l_D(t)$ = path length traveled by the neutron in the detector, expressed in terms of the apparent flight time.

The term

$$d\vec{\Omega} = \frac{\hat{i}' \cdot \vec{\Omega}}{l_f^2} dA_D$$

is the element of solid angle subtended by an element of detector front surface at the interaction in the target $P_T(x,y)$. The distance from P_T to a point on the face of the detector is l_f.

For given neutron energies, v_n and $\Sigma(v_n)$ are constants. If $\Sigma_p(v_p; v_n, \oplus)$ does not vary too rapidly with $\oplus$ or v_p, it may also be considered to be constant. Experiments are normally designed to make these assumptions valid.

The distance traveled by the neutron from its birth point in the target, $P_T(x,y)$, to the point of detection, P_D, is $t_n v_n$. With the aid of Eq. (2),

$$l_f + l_D = (t - t_p - t_c) v_n \ . \tag{8}$$

Considering only light rays which are normal to the photocathode,

$$t_c = \frac{K}{c}[D - l_D(\hat{i}' \cdot \vec{\Omega})] \ , \tag{9}$$

when

K = index of refraction of the detector,
c = speed of light,
D = thickness of the detector.

Substituting Eq. (9) into Eq. (8) and solving for l_D yields

$$l_D = \frac{(t - t_p)v_n - (KD\, v_n/c) - l_f}{1 - K(\hat{i}' \cdot \vec{\Omega})\,(v_n/c)} \ . \tag{10}$$

The incident proton loses energy in the target through numerous atomic collisions. If the time reference is taken at $x = 0$ with the target imagined to be absent,

$$t_p = \frac{x}{v_p} + \frac{X^2}{4E_p v_p}\left(-\frac{dE}{dx}\right) , \tag{11}$$

where

v_p = proton velocity,
E_p = proton energy,
$-dE/dx$ = incremental energy loss per unit path length for protons in the target material ($-dE/dx$ is a positive number).

For neutron velocities which approach 160 MeV, the response function is sharply peaked. To more easily define the overall shape of the distribution, a convolution of the timing jitter distribution is performed with $E_\oplus(t,X,x,v_n)$. (Otherwise this jitter must be introduced later in the calculation.) The jitter distribution $J(t_j)$ is assumed to be normal. Then in Eq. (3), $E_\oplus(t,X,x,v_n)$ is just replaced by $F_\oplus(t_i,X,x,v_n)$, where

$$F_\oplus(t_i,X,x,v_n)\,dt_i = dt_i \int_t E_\oplus(t,X,x,v_n)\,J(t_i - t)\,dt \tag{12}$$

and $C(t,v_n)$ is correspondingly replaced by $G(t_i,v_n)$.

Computer programs are now being written to evaluate $G(t_i,v_n)$. Upon completion of this evaluation, the result will be combined with a pulse-height spectrum in order to estimate the time dispersion from the pulse-height-dependent time slewing. When the time analyzer response is also included, this will yield the overall time response function for the spectrometer.

References

[1]Partially funded by the National Aeronautics and Space Administration under NASA order R-104(1).

[2]R. W. Peelle, T. A. Love, and G. A. Luce, *Neutron Phys. Div. Ann. Progr. Rept. Sept. 1, 1962*, ORNL-3360, p. 286.

[3]R. T. Santoro, *Neutron Phys. Div. Ann. Progr. Rept. Aug. 1, 1965*, ORNL-3858, vol. II, p. 86.

9.6 PROTON RECOIL SPECTROMETER FOR NEUTRON SPECTRA BETWEEN 50 AND 450 MeV[1]

W. A. Gibson — J. W. Wachter
W. R. Burrus — C. F. Johnson[2]

A proton recoil spectrometer has been constructed and used to obtain energy spectra of neutrons emitted from targets bombarded by 160- and 450-MeV protons. The instrument employs a polyethylene radiator as the source of the recoil protons

and measures the energy of the protons from the pulse height obtained when the proton passes through a thin NaI(Tl) crystal. The paper discusses the details of constructing the spectrometer and the circuitry used during operation. A Monte Carlo program for calculating the efficiency and resolution of the spectrometer is described. The effect of the Landau spread in the energy deposited in the NaI(Tl) energy detector is included in the resolution calculation. Typical energy spectra for secondary neutrons and protons are presented, and the unfolding program used to compensate for the skewed energy resolution function of the spectrometer is discussed.

References

[1]Abstract of ORNL-TM-1525 (June 1966); also to be published in *Nuclear Instruments and Methods*. Work partially funded by the National Aeronautics and Space Administration under NASA order R-104(1).

[2]General Dynamics, Fort Worth, Texas.

INTERNAL DISTRIBUTION

1. L. S. Abbott
2. P. M. Aebersold
3. F. S. Alsmiller
4. R. G. Alsmiller, Jr.
5. J. Barish (K-25)
6. H. W. Bertini
7. F. E. Bertrand
8. T. V. Blosser
9. R. T. Boughner
10. W. R. Burrus
11. V. R. Cain
12. A. D. Callihan
13. Y. Cassagsnou
14. G. T. Chapman
15. H. C. Claiborne
16. F. H. S. Clark
17. C. E. Clifford
18. W. Coleman
19. R. R. Coveyou
20. G. de Saussure
21. J. K. Dickens
22. L. Dresner
23. J. F. Ellis
24. M. M. El-Shishini
25. R. J. Fox
26. R. M. Freestone, Jr.
27. W. A. Gibson
28. F. E. Gillespie
29. L. W. Gilley
30. J. H. Gillette
31. J. Gurney (K-25)
32. M. Guthrie
33. R. Gwin
34. V. M. Hamrick
35. M. V. Harlow
36. M. P. Haydon
37. K. M. Henry, Jr.
38. N. W. Hill
39. L. B. Holland
40. J. L. Hull
41. D. Irving
42. E. B. Johnson
43. W. H. Jordan
44. D. T. King
45. W. E. Kinney
46. C. E. Larson
47. J. Lewin
48. A. Lottin
49. T. A. Love
50. J. J. Lynn
51. H. G. MacPherson
52. R. E. Maerker
53. D. W. Magnuson
54–78. F. C. Maienschein
79. J. J. Manning
80. B. F. Maskewitz
81. J. W. McConnell
82. J. T. Mihalczo
83. B. McGill
84. H. S. Moran
85. F. J. Muckenthaler
86–87. R. B. Parker
88. R. W. Peelle
89. S. K. Penny
90. C. M. Perey
91. F. G. Perey
92. S. J. Raffety
93. E. R. Rohrer
94. R. Rust (K-25)
95. R. T. Santoro
96. W. Scott
97. E. G. Silver
98. M. J. Skinner
99. E. A. Straker
100. J. T. Thomas
101. J. H. Todd
102. D. K. Trubey
103. W. C. Tunnell
104. V. V. Verbinski
105. J. Wachter
106. D. R. Ward
107. J. W. Webster
108. A. M. Weinberg
109. L. W. Weston
110. G. C. Williams
111. G. Young
112. M. Young
113. K. J. Yost
114. W. Zobel
115. G. Dessauer (Consultant)
116. B. C. Diven (Consultant)
117. M. L. Goldberger (Consultant)

118. M. H. Kalos (Consultant)
119. L. V. Spencer (Consultant)
120. Radiation Shielding Information Center
121. Biology Library
122–124. Central Research Library
125. Reactor Division Library
126–127. ORNL-Y-12 Technical Library, Document Reference Section
128–387. Laboratory Records Department
388. Laboratory Records, ORNL R.C.

EXTERNAL DISTRIBUTION

389. Research and Development Division, AEC, ORO
390. J. A. Swartout, 270 Park Avenue, New York, New York
391. W. W. Grigorieff, Assistant to the Executive Director, Oak Ridge Associated Universities
392–763. Given distribution as shown in TID-4500 under Physics category (75 copies – CFSTI)